A 27-point scheme for a 3D frequency-domain scalar wave equation based on an average-derivative method

Jing-Bo Chen*

Key Laboratory of Petroleum Resources Research, Institute of Geology and Geophysics, Chinese Academy of Sciences, P. O. Box 9825, Beijing 100029, China

ABSTRACT

Based on an average-derivative method and optimization techniques, a 27-point scheme for a 3D frequency-domain scalar wave equation is developed. Compared to the rotated-coordinate approach, the average-derivative optimal method is not only concise but also applies to equal and unequal directional sampling intervals. The resulting 27-point scheme uses a 27-point operator to approximate spatial derivatives and the mass acceleration term. The coefficients are determined by minimizing phase velocity dispersion errors and the resultant optimal coefficients depend on ratios of directional sampling intervals. Compared to the classical 7-point scheme, the number of grid points per shortest wavelength is reduced from approximately 13 to approximately 4 by this 27-point optimal scheme for equal directional sampling intervals and unequal directional sampling intervals as well. Two numerical examples are presented to demonstrate the theoretical analysis. The average-derivative algorithm is also extended to a 3D frequency-domain viscous scalar wave equation.

Key words: Scalar wave equation, Average-derivative method.

INTRODUCTION

Recently, full-waveform inversion (FWI) has been attracting increasing attention in the community of exploration geophysics. FWI is a full-wavefield-modelling-based data-fitting process to extract structural information of the subsurface from seismograms (Tarantola 1984; Gauthier, Virieux and Tarantola 1986; Pratt and Worthington 1990; Pratt, Shin and Hicks 1998; Boonyasiriwat *et al.* 2009; Virieux and Operto 2009). Forward modelling constitutes an important part of FWI. Forward modelling can be classified into two categories: time-domain modelling and frequency-domain modelling. Compared to time-domain modeling (Chen 2009), frequency-domain modelling has its advantages: convenient manipulations of a single frequency, multi-shot computation based on a direct solver and easy implementation of attenuation (Jo, Shin and Suh 1996). Another advantage of frequency-domain modelling is also worth mentioning. No wavefield-

storage issue occurs when constructing the gradient of FWI for frequency-domain modelling. This is not the case when constructing the gradient of FWI for time-domain modelling. This is because the forward source wavefield and backward receiver wavefield are computed in the opposite time direction (Symes 2007; Clapp 2009).

The main disadvantage of frequency-domain modelling is that it can be only performed in an implicit way by solving a set of linear equations. In comparison with time-domain modelling, this disadvantage is particularly obvious when it comes to 3D computation. Therefore, reducing the number of grid points per shortest wavelength is in great demand in particular when direct solution techniques are employed. Using a rotated coordinate system, Jo *et al.* (1996) developed a 9-point operator to approximate the Laplacian and the mass acceleration terms in a 2D scalar wave equation. The coefficients are determined by obtaining the best normalized phase velocity dispersion curves. This 9-point scheme reduces the number of grid points per wavelength to approximately 4 and leads to significant reductions of computer memory and CPU time.

---

*E-mail: chenjb@mail.iggcas.ac.cn

Hustedt, Operto and Virieux (2004) and Operto, Virieux and Sourbier (2007) generalized the rotated-coordinate method to a variable density case and a 3D case, respectively.

A disadvantage of the rotated-coordinate method is that equal directional sampling intervals are required. To overcome the disadvantage of the rotated optimal 9-point scheme, Chen (2012) developed a new 9-point finite-difference scheme for a 2D scalar wave equation based on an average-derivative approach (Chen 2001; Chen 2008). This new scheme imposes no restriction of equal directional sampling intervals and reduces the number of grid points per shortest wavelength to approximately 4 for both equal and unequal directional sampling intervals. Furthermore, due to its flexibility and simplicity, the average-derivative method can be easily extended to the viscous scalar wave equation and 3D wave equation.

In Chen (2012) the average-derivative method was discussed mainly in terms of a 2D frequency-domain scalar wave equation and the 3D case was only briefly examined. In fact, the average-derivative method for a 3D wave equation is more attractive because it is not only concise but also applies to both equal and unequal directional sampling intervals. On the other hand, the construction of 3D finite-difference schemes based on the rotated-system approach is not only very complicated but also restricted to equal directional sampling intervals because a lot of coordinate-transformations based on equal grid directional intervals are needed. The present paper is a further development of Chen (2012) and I will explore the average-derivative method for a 3D frequency-domain scalar wave equation in detail, including coefficients optimization, dispersion analysis, generalization and numerical examples.

A 27-POINT SCHEME FOR A 3D WAVE EQUATION

The 3D frequency-domain scalar wave equation reads:

$$\frac{\partial^2 P}{\partial x^2} + \frac{\partial^2 P}{\partial y^2} + \frac{\partial^2 P}{\partial z^2} + \frac{\omega^2}{v^2} P = 0, \qquad (1)$$

where P is the pressure wavefield, ω is the circular frequency and $v(x, y, z)$ is the velocity.

A classical 7-point scheme for equation (1) is (see Fig. 1 a):

$$\frac{P_{m+1,l,n} - 2P_{m,l,n} + P_{m-1,l,n}}{\Delta x^2} + \frac{P_{m,l+1,n} - 2P_{m,l,n} + P_{m,l-1,n}}{\Delta y^2}$$

$$+ \frac{P_{m,l,n+1} - 2P_{m,l,n} + P_{m,l,n-1}}{\Delta z^2} + \frac{\omega^2}{v_{m,l,n}^2} P_{m,l,n} = 0, \qquad (2)$$

where $P_{m,l,n} \approx P(m\Delta x, l\Delta y, n\Delta z)$, $v_{m,l,n} \approx v(m\Delta x, l\Delta y, n\Delta z)$ and Δx, Δy and Δz are directional sampling intervals in the x-, y- and z-directions, respectively.

As can be seen later, within the phase velocity error of 1%, the classical 7-point scheme (2) requires approximately 13 grid points per shortest wavelength. In order to reduce the numerical dispersion of scheme (2), very fine grids are required. This leads to a huge amount of computer storage and CPU time. Therefore, reducing the number of grid points required per shortest wavelength is needed.

To this aim, Chen (2012) developed an average-derivative approach. Using a weighted-average technique, the average-derivative method provides a family of approximations to derivatives from which the optimization approximation can be determined to greatly improve dispersion accuracy. This method is particularly advantageous when it comes to the 3D frequency-domain wave equation because no complicated coordinate transforms are needed.

An average-derivative optimal 27-point scheme for equation (1) can be obtained as follows (see Fig. 1 b):

$$\frac{\bar{P}_{m+1,l,n} - 2\bar{P}_{m,l,n} + \bar{P}_{m-1,l,n}}{\Delta x^2} + \frac{\hat{P}_{m,l+1,n} - 2\hat{P}_{m,l,n} + \hat{P}_{m,l-1,n}}{\Delta y^2}$$

$$+ \frac{\tilde{P}_{m,l,n+1} - 2\tilde{P}_{m,l,n} + \tilde{P}_{m,l,n-1}}{\Delta z^2}$$

$$+ \frac{\omega^2}{v_{m,l,n}^2}(cP_{m,l,n} + dA + eB + fC) = 0, \qquad (3)$$

where

$$\bar{P}_{r,l,n} = \alpha_1(P_{r,l+1,n} + P_{r,l,n+1} + P_{r,l-1,n} + P_{r,l,n-1})$$

$$+ \alpha_2(P_{r,l+1,n+1} + P_{r,l-1,n+1} + P_{r,l+1,n-1} + P_{r,l-1,n-1})$$

$$+ (1 - 4\alpha_1 - 4\alpha_2)P_{r,l,n}, \qquad r = m+1, m, m-1,$$

$$\hat{P}_{m,s,n} = \beta_1(P_{m+1,s,n} + P_{m,s,n+1} + P_{m-1,s,n} + P_{m,s,n-1})$$

$$+ \beta_2(P_{m+1,s,n+1} + P_{m+1,s,n-1} + P_{m-1,s,n+1} + P_{m-1,s,n-1})$$

$$+ (1 - 4\beta_1 - 4\beta_2)P_{m,s,n}, \qquad s = l+1, l, l-1,$$

$$\tilde{P}_{m,l,q} = \gamma_1(P_{m+1,l,q} + P_{m,l+1,q} + P_{m-1,l,q} + P_{m,l-1,q})$$

$$+ \gamma_2(P_{m+1,l+1,q} + P_{m+1,l-1,q} + P_{m-1,l+1,q} + P_{m-1,l-1,q})$$

$$+ (1 - 4\gamma_1 - 4\gamma_2)P_{m,l,q}, \qquad q = n+1, n, n-1,$$

$$A = (P_{m,l+1,n} + P_{m,l,n+1} + P_{m,l-1,n} + P_{m,l,n-1})$$

$$+ (P_{m+1,l,n} + P_{m-1,l,n}),$$

$$B = (P_{m+1,l+1,n} + P_{m+1,l,n+1} + P_{m+1,l-1,n} + P_{m+1,l,n-1}$$

$$+ P_{m-1,l+1,n} + P_{m-1,l,n+1} + P_{m-1,l-1,n} + P_{m-1,l,n-1}$$

$$+ P_{m,l+1,n+1} + P_{m,l-1,n+1}) + P_{m,l+1,n-1} + P_{m,l-1,n-1},$$
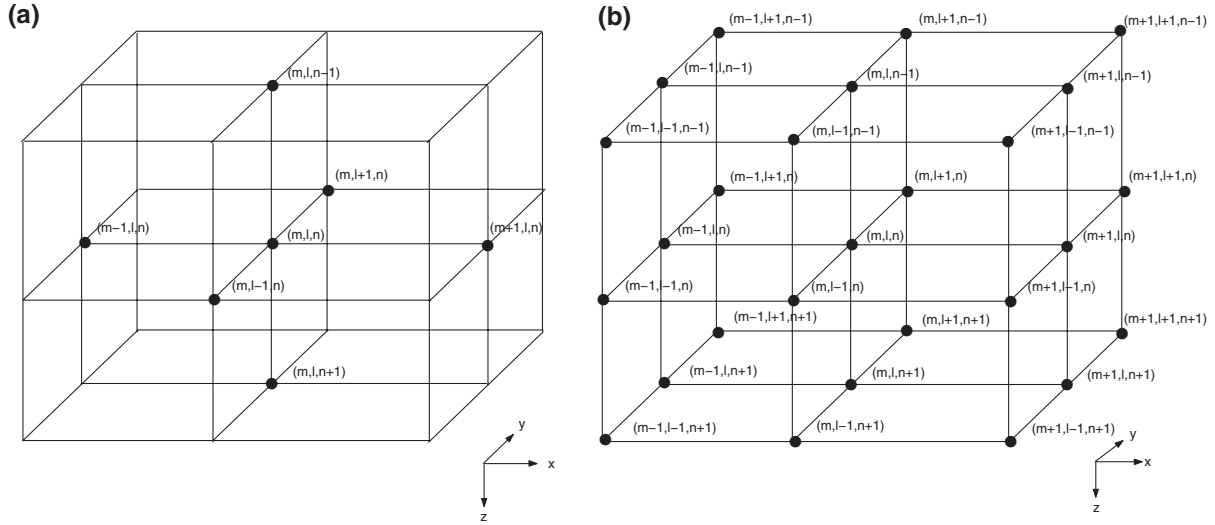
(a)

(b)

Figure 1 Schematic of the classical 7-point scheme (a) and the average-derivative optimal 27-point scheme (b).

$$C = (P_{m+1, l+1, n+1} + P_{m+1, l-1, n+1} + P_{m+1, l+1, n-1}$$

$$+ P_{m+1, l-1, n-1} + P_{m-1, l+1, n+1} + P_{m-1, l-1, n+1}$$

$$+ P_{m-1, l+1, n-1} + P_{m-1, l-1, n-1}),$$

where α_1, α_2, β_1, β_2, γ_1, γ_2, c, d and e are coefficients and $f = \frac{1-c-6d-12e}{8}$.

In equation (3), the approximations of the derivatives are weighted averages of three kinds of approximations and therefore, I call equation (3) the average-derivative optimal 27-point scheme. The motivation of the average-derivative method is to provide a family of approximations to the derivatives from which the optimization approximation can be chosen to reduce dispersion errors (Chen 2012). Compared to the 3D scheme based on the rotated-coordinate method (Operto *et al.* 2007), the average-derivative 27-point scheme (3) is not only concise but also applies to the situation where the directional sampling intervals Δx, Δy, and Δz are different.

In addition, the average-derivative optimal 27-point scheme (3) also includes the classical 7-point scheme as a special case, because when $\alpha_1 = 0$, $\alpha_2 = 0$, $\beta_1 = 0$, $\beta_2 = 0$, $\gamma_1 = 0$, $\gamma_2 = 0$, $c = 1$, $d = 0$ and $e = 0$, scheme (3) becomes scheme (2).

OPTIMIZATION AND DISPERSION ANALYSIS

In this section, I perform optimization of coefficients of the average-derivative optimal 27-point scheme (3) and make cor-

responding dispersion analysis. Substituting $P(x, y, z, \omega) = P_0 e^{-i(k_x x + k_y y + k_z z)}$ into equation (3) and assuming a constant v, one obtains the discrete dispersion relation:

$$\frac{\omega^2}{v^2} =$$

$$\frac{4 \sin^2\left(\frac{k_x \Delta x}{2}\right) E_x + 4 r_1^2 \sin^2\left(\frac{k_y \Delta y}{2}\right) E_y + 4 r_2^2 \sin^2\left(\frac{k_z \Delta z}{2}\right) E_z}{\Delta x^2 (c + 2d \tilde{A} + 4e \tilde{B} + 8 f \tilde{C})}, \quad (4)$$

where

$$E_x = 2\alpha_1 (\cos(k_y \Delta y) + \cos(k_z \Delta z))$$
$$+ 4\alpha_2 \cos(k_y \Delta y) \cos(k_z \Delta z) + (1 - 4\alpha_1 - 4\alpha_2),$$

$$E_y = 2\beta_1 (\cos(k_x \Delta x) + \cos(k_z \Delta z))$$
$$+ 4\beta_2 \cos(k_x \Delta x) \cos(k_z \Delta z) + (1 - 4\beta_1 - 4\beta_2),$$

$$E_z = 2\gamma_1 (\cos(k_x \Delta x) + \cos(k_y \Delta y))$$
$$+ 4\gamma_2 \cos(k_x \Delta x) \cos(k_y \Delta y) + (1 - 4\gamma_1 - 4\gamma_2),$$

$$r_1 = \frac{\Delta x}{\Delta y}, \quad r_2 = \frac{\Delta x}{\Delta z},$$

$$\tilde{A} = \cos(k_x \Delta x) + \cos(k_y \Delta y) + \cos(k_z \Delta z),$$

$$\tilde{B} = \cos(k_x \Delta x) \cos(k_y \Delta y) + \cos(k_x \Delta x) \cos(k_z \Delta z)$$
$$+ \cos(k_y \Delta y) \cos(k_z \Delta z),$$

$$\tilde{C} = \cos(k_x \Delta x) \cos(k_y \Delta y) \cos(k_z \Delta z).$$

In equation (4), I suppose that $\Delta x = \max\{\Delta x, \Delta y, \Delta z\}$. For other cases, a similar analysis can be performed. If $\Delta y = \max\{\Delta x, \Delta y, \Delta z\}$, r_1 and r_2 should be defined by $r_1 = \frac{\Delta y}{\Delta x}$

Table 1 Optimization coefficients for α_1, α_2, β_1, β_2, γ_1, γ_2, c, d and e.

	α_1	α_2	β_1	β_2	γ_1	γ_2	c	d	e
$r_1 = 1$ $r_2 = 1$	0.097426	0.001449	0.042419	0.028953	0.100520	0.000000	0.474309	0.084057	0.001779
$r_1 = 1$ $r_2 = 2$	0.027756	0.035823	0.099402	0.000000	0.075170	0.010711	0.468043	0.086909	0.000875
$r_1 = 1$ $r_2 = 3$	0.091501	0.005050	0.101582	0.000000	0.062715	0.016398	0.454915	0.090845	0.000000
$r_1 = 2$ $r_2 = 1$	0.070821	0.015683	0.063389	0.017191	0.099169	0.001626	0.4531125	0.091146	0.000000
$r_1 = 2$ $r_2 = 2$	0.063269	0.007299	0.000762	0.049544	0.091669	0.004497	0.461498	0.089750	0.000000
$r_1 = 2$ $r_2 = 3$	0.036872	0.015865	0.060604	0.022265	0.012939	0.042942	0.456929	0.090512	0.000000

and $r_2 = \frac{\Delta y}{\Delta z}$, respectively. If $\Delta z = \max\{\Delta x, \Delta y, \Delta z\}$, r_1 and r_2 should be defined by $r_1 = \frac{\Delta z}{\Delta x}$ and $r_2 = \frac{\Delta z}{\Delta y}$, respectively.

From equation (4), the normalized phase velocity can be derived as follows:

$$\frac{V_{ph}}{v} = \frac{\left\{\sin^2\left(\frac{\pi \sin\theta\cos\phi}{G}\right)E_x + r_1^2\sin^2\left(\frac{\pi \sin\theta\sin\phi}{r_1 G}\right)E_y + r_2^2\sin^2\left(\frac{\pi \cos\theta}{r_2 G}\right)E_z\right\}^{\frac{1}{2}}}{\frac{\pi}{G}\{c + 2d\tilde{A} + 4e\tilde{B} + 8f\tilde{C}\}^{\frac{1}{2}}},$$

(5)

where V_{ph} is the phase velocity, $k_x = k\sin\theta\cos\phi$, $k_y = k\sin\theta\sin\phi$, $k_z = k\cos\theta$, $G = \frac{2\pi}{k\Delta x}$, θ is the propagation angle, ϕ is the azimuth angle and

$$E_x = 2\alpha_1\left(\cos\left(\frac{2\pi\sin\theta\sin\phi}{r_1 G}\right) + \cos\left(\frac{2\pi\cos\theta}{r_2 G}\right)\right)$$
$$+ 4\alpha_2\cos\left(\frac{2\pi\sin\theta\sin\phi}{r_1 G}\right)\cos\left(\frac{2\pi\cos\theta}{r_2 G}\right)$$
$$+ (1 - 4\alpha_1 - 4\alpha_2),$$

$$E_y = 2\beta_1\left(\cos\left(\frac{2\pi\sin\theta\cos\phi}{G}\right) + \cos\left(\frac{2\pi\cos\theta}{r_2 G}\right)\right)$$
$$+ 4\beta_2\cos\left(\frac{2\pi\sin\theta\cos\phi}{G}\right)\cos\left(\frac{2\pi\cos\theta}{r_2 G}\right)$$
$$+ (1 - 4\beta_1 - 4\beta_2),$$

$$E_z = 2\gamma_1\left(\cos\left(\frac{2\pi\sin\theta\cos\phi}{G}\right) + \cos\left(\frac{2\pi\sin\theta\sin\phi}{r_1 G}\right)\right)$$
$$+ 4\gamma_2\cos\left(\frac{2\pi\sin\theta\cos\phi}{G}\right)\cos\left(\frac{2\pi\sin\theta\sin\phi}{r_1 G}\right)$$
$$+ (1 - 4\gamma_1 - 4\gamma_2),$$

$$\tilde{A} = \cos\left(\frac{2\pi\sin\theta\cos\phi}{G}\right) + \cos\left(\frac{2\pi\sin\theta\sin\phi}{r_1 G}\right)$$

$$+ \cos\left(\frac{2\pi\cos\theta}{r_2 G}\right),$$

$$\tilde{B} = \cos\left(\frac{2\pi\sin\theta\cos\phi}{G}\right)\cos\left(\frac{2\pi\sin\theta\sin\phi}{r_1 G}\right)$$
$$+ \cos\left(\frac{2\pi\sin\theta\cos\phi}{G}\right)\cos\left(\frac{2\pi\cos\theta}{r_2 G}\right)$$
$$+ \cos\left(\frac{2\pi\sin\theta\sin\phi}{r_1 G}\right)\cos\left(\frac{2\pi\cos\theta}{r_2 G}\right),$$

$$\tilde{C} = \cos\left(\frac{2\pi\sin\theta\cos\phi}{G}\right)\cos\left(\frac{2\pi\sin\theta\sin\phi}{r_1 G}\right)$$
$$\times \cos\left(\frac{2\pi\cos\theta}{r_2 G}\right).$$

In equation (5), if $\Delta y = \max\{\Delta x, \Delta y, \Delta z\}$, G should be defined by $G = \frac{2\pi}{k\Delta y}$. If $\Delta z = \max\{\Delta x, \Delta y, \Delta z\}$, G should be defined by $G = \frac{2\pi}{k\Delta z}$.

The coefficients α_1, α_2, β_1, β_2, γ_1, γ_2, c, d and e are determined by minimizing the phase error:

$$PE = \iiint\left[1 - \frac{V_{ph}(\theta, \phi, \tilde{k}; \alpha_1, \alpha_2, \beta_1, \beta_2, \gamma_1, \gamma_2, c, d, e)}{v}\right]^2$$
$$\times d\tilde{k}d\theta d\phi,$$

(6)

where $\tilde{k} = \frac{1}{G}$.

The ranges of $\tilde{k}$, θ and ϕ are taken as $[0, 0.25]$, $[0, \frac{\pi}{2}]$ and $[0, \frac{\pi}{2}]$, respectively. The range of $\tilde{k}$ depends on the number of grid points involved in the scheme. The more grid points are involved, the larger the range of $\tilde{k}$ can be taken. For scheme (3), the range $[0, 0.25]$ is a reasonable choice and a larger range can lead to a degradation of dispersion accuracy.

A constrained non-linear optimization program `fmincon` in **Matlab** is used to determine the optimization coefficients. The optimization coefficients for different $r_1 = \frac{\Delta x}{\Delta y}$ and
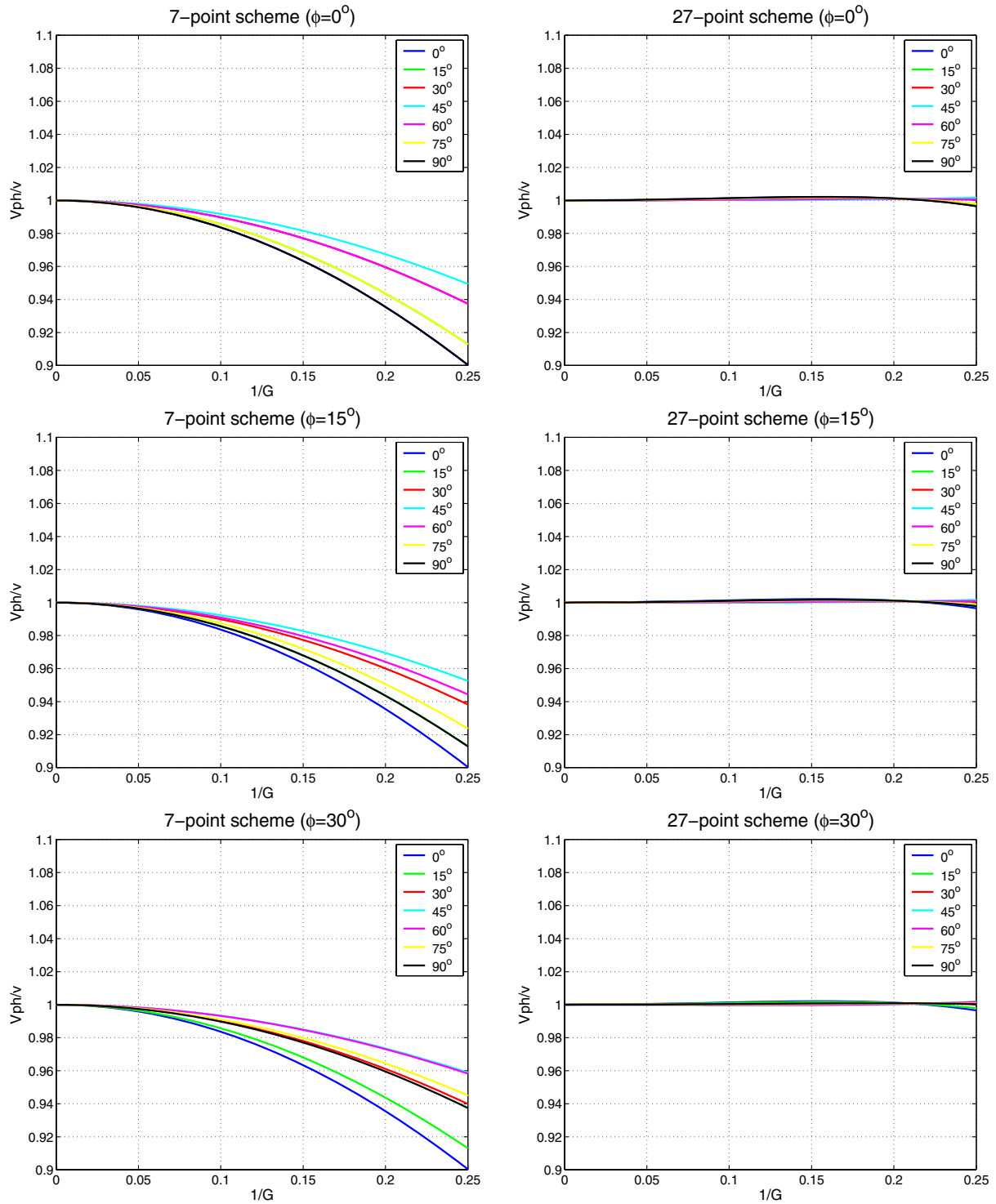
Figure 2 Normalized phase velocity curves of the classical 7-point scheme and the average-derivative optimal 27-point scheme for fixed azimuth angle ϕ and different propagation angles θ when $r_1 = 1$ and $r_2 = 1$.

Figure 3 Continuation of Fig. 2.

Figure 4 Normalized phase velocity curves of the classical 7-point scheme and the average-derivative optimal 27-point scheme for fixed propagation angle θ and different azimuth angles ϕ when $r_1 = 1$ and $r_2 = 1$.

Figure 5 Continuation of Fig. 4.

(a)

(b)
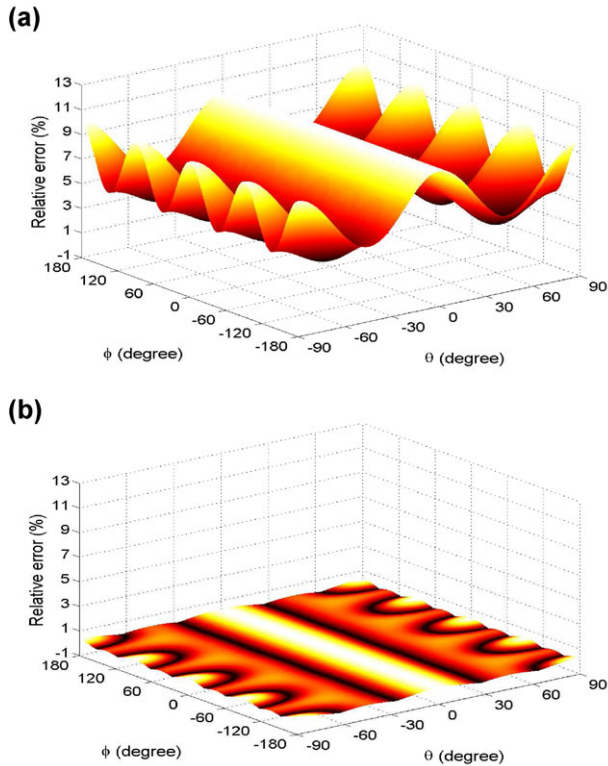
Figure 6 The relative phase velocity error for the classical 7-point scheme (a) and the average-derivative optimal 27-point scheme (b) when $r_1 = 1$ and $r_2 = 1$.

$r_2 = \frac{\Delta x}{\Delta z}$ when $\Delta x = \max\{\Delta x, \Delta y, \Delta z\}$ are listed in Table 1. One can see that the coefficients $\alpha_1, \alpha_2, \beta_1, \beta_2, \gamma_1, \gamma_2$ and e vary with r_1 and r_2 and the changes in coefficients c and d are small.

I now perform numerical dispersion analysis. First, I consider the case where $r_1 = 1$ and $r_2 = 1$, which corresponds to the equal directional intervals $\Delta x = \Delta y = \Delta z$. Figures 2 and 3 show normalized phase velocity curves of the classical 7-point scheme (2) and the average-derivative optimal 27-point scheme (3) for fixed azimuth angle ϕ and different propagation angles θ. Figures 4 and 5 show normalized phase velocity curves of the classical 7-point scheme (2) and the average-derivative optimal 27-point scheme (3) for fixed propagation angle θ and different azimuth angles ϕ. From these figures, one can conclude that within the phase velocity error of 1%, the classical 7-point scheme (2) requires approximately 13 grid points per shortest wavelength, while the average-derivative optimal 27-point scheme (3) requires approximately 4 points.

In order to obtain an overall estimation of the phase velocity errors varying with ϕ and θ, Fig. 6 shows the following relative phase velocity error:

$$RE = \left| \frac{V_{pb}(\phi, \theta, G) - v}{v} \right|, \quad -180^\circ \leqslant \phi \leqslant 180^\circ,$$
$$-90^\circ \leqslant \theta \leqslant 90^\circ \text{ and } G = 4. \quad (7)$$

For the classical 7-point scheme (2), the maximum relative error is 9.97% while for the average-derivative optimal 27-point scheme (3), the maximum relative error is 0.3%.

Second, I consider the case where $r_1 = 2$ and $r_2 = 3$, which corresponds to the unequal directional intervals $\Delta x = 2\Delta y = 3\Delta z$. Figures 7 and 8 show normalized phase velocity curves of the classical 7-point scheme (2) and the average-derivative optimal 27-point scheme (3) for fixed azimuth angle ϕ and different propagation angles θ. Figures 9 and 10 show normalized phase velocity curves of the classical 7-point scheme (2) and the average-derivative optimal 27-point scheme (3) for fixed propagation angle θ and different azimuth angles ϕ. From these figures, one can conclude that within the phase velocity error of 1%, the classical 7-point scheme (2) requires approximately 13 grid points per shortest wavelength, while the average-derivative optimal 27-point scheme (3) requires approximately 4 points.

Figure 11 shows the relative phase velocity error (equation (7)). For the classical 7-point scheme (2), the maximum relative error is 9.97% while for the average-derivative optimal 27-point scheme (3), the maximum relative error is 0.5%.

For other cases on r_1 and r_2, a similar analysis can be made. The common conclusion is that within the phase velocity error of 1% and for equal and unequal directional sampling intervals, the classical 7-point scheme (2) requires approximately 13 grid points per shortest wavelength, while the average-derivative optimal 27-point scheme (3) requires approximately 4 grid points.

GENERALIZATION OF SCHEME(3)

Due to its flexibility and simplicity, scheme (3) can be easily extended to the 3D viscous scalar wave equation.

The 3D viscous scalar wave equation reads:

$$\frac{\partial}{\partial x}\left(\frac{1}{\rho}\frac{\partial P}{\partial x}\right) + \frac{\partial}{\partial y}\left(\frac{1}{\rho}\frac{\partial P}{\partial y}\right) + \frac{\partial}{\partial z}\left(\frac{1}{\rho}\frac{\partial P}{\partial z}\right) + \frac{\omega^2}{\kappa}P = 0, \quad (8)$$

Figure 7 Normalized phase velocity curves of the classical 7-point scheme and the average-derivative optimal 27-point scheme for fixed azimuth angle ϕ and different propagation angles θ when $r_1 = 2$ and $r_2 = 3$.
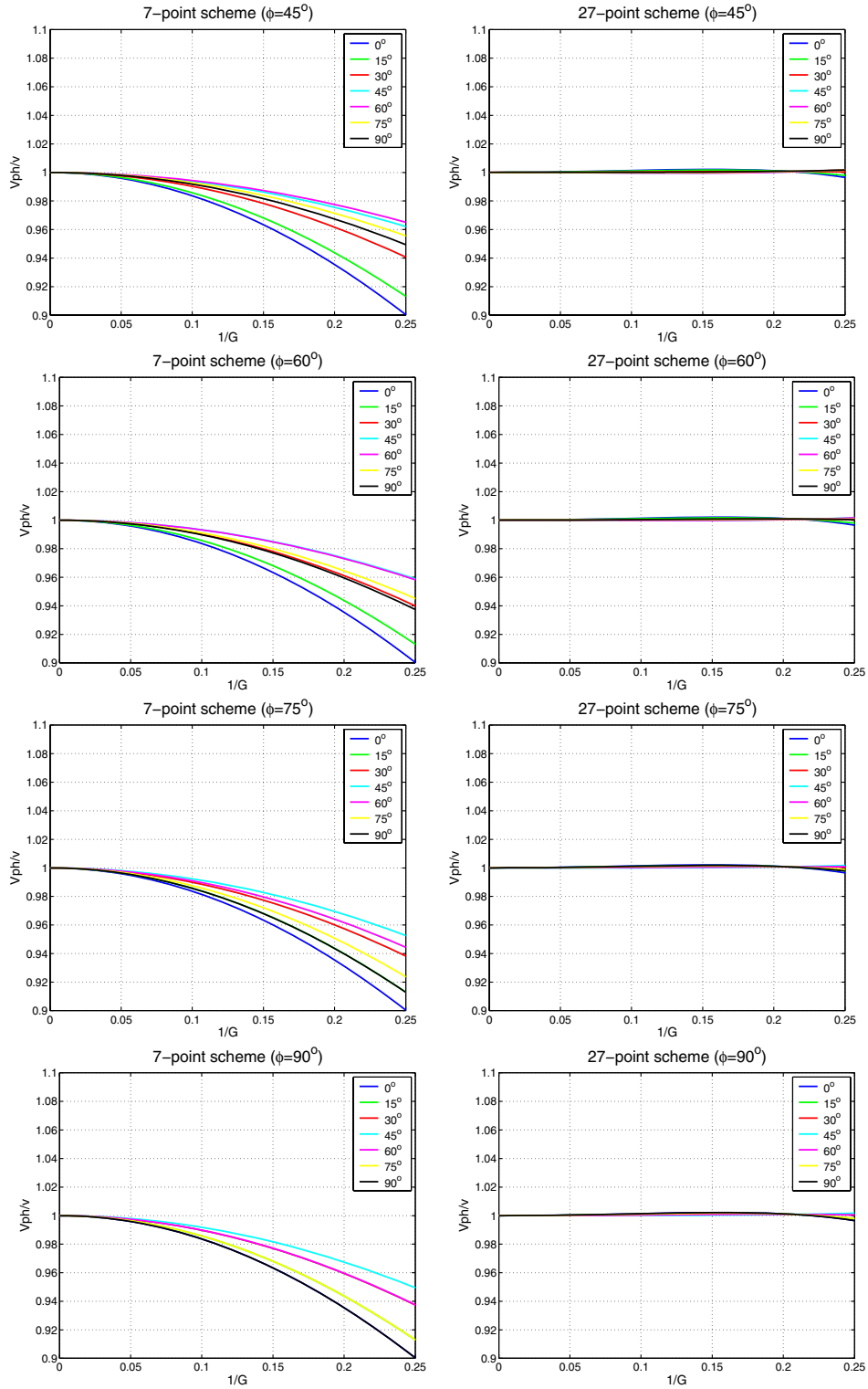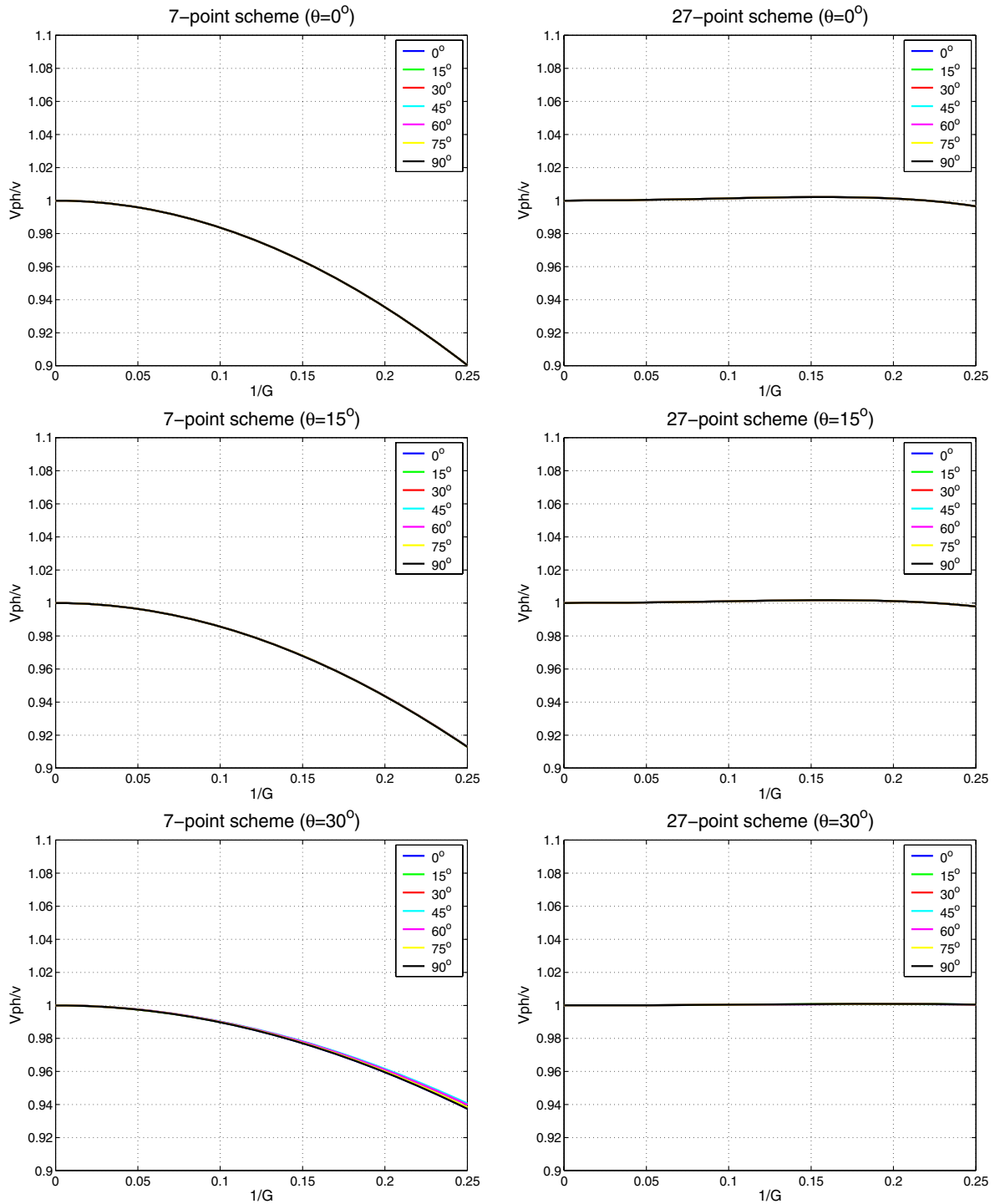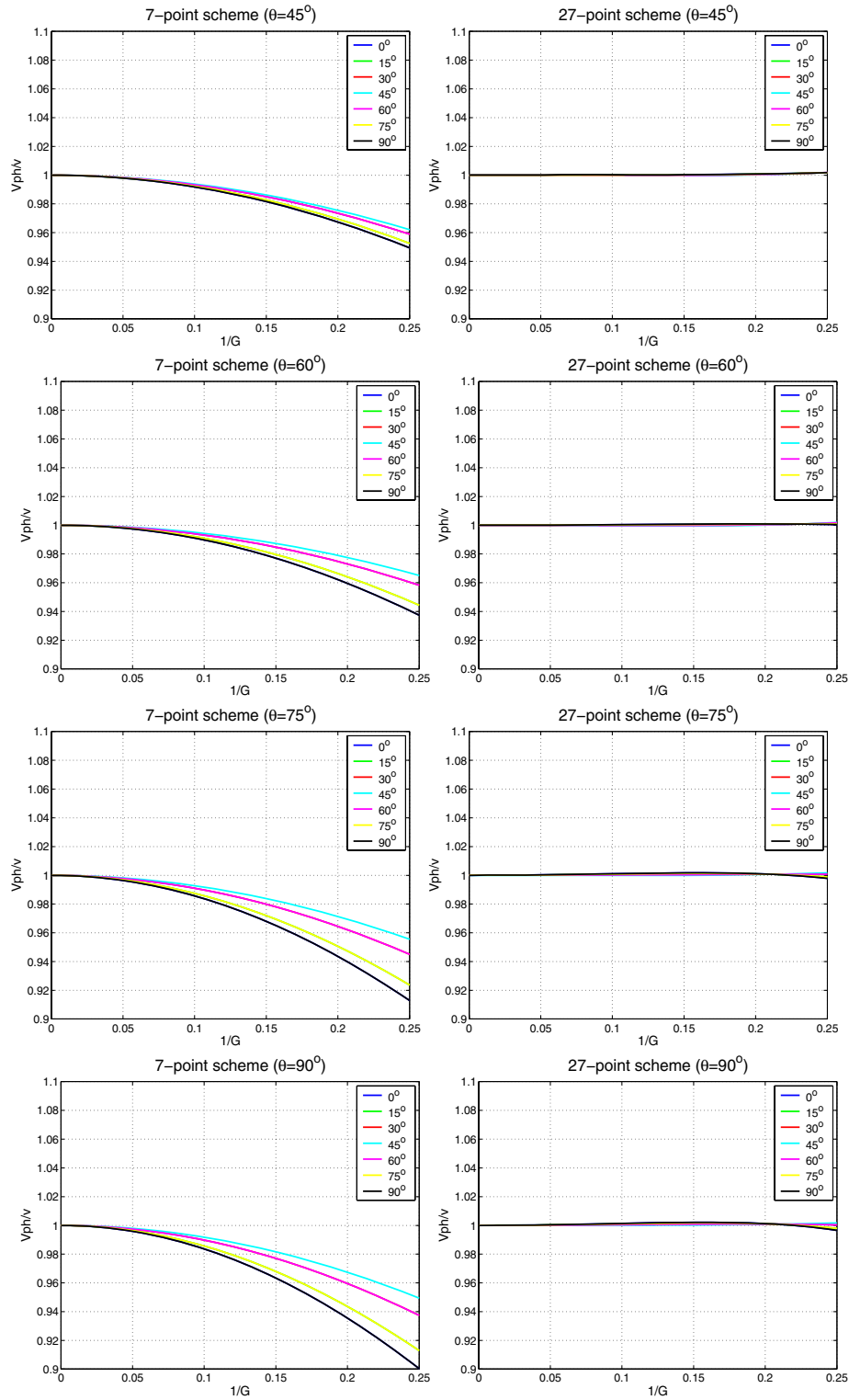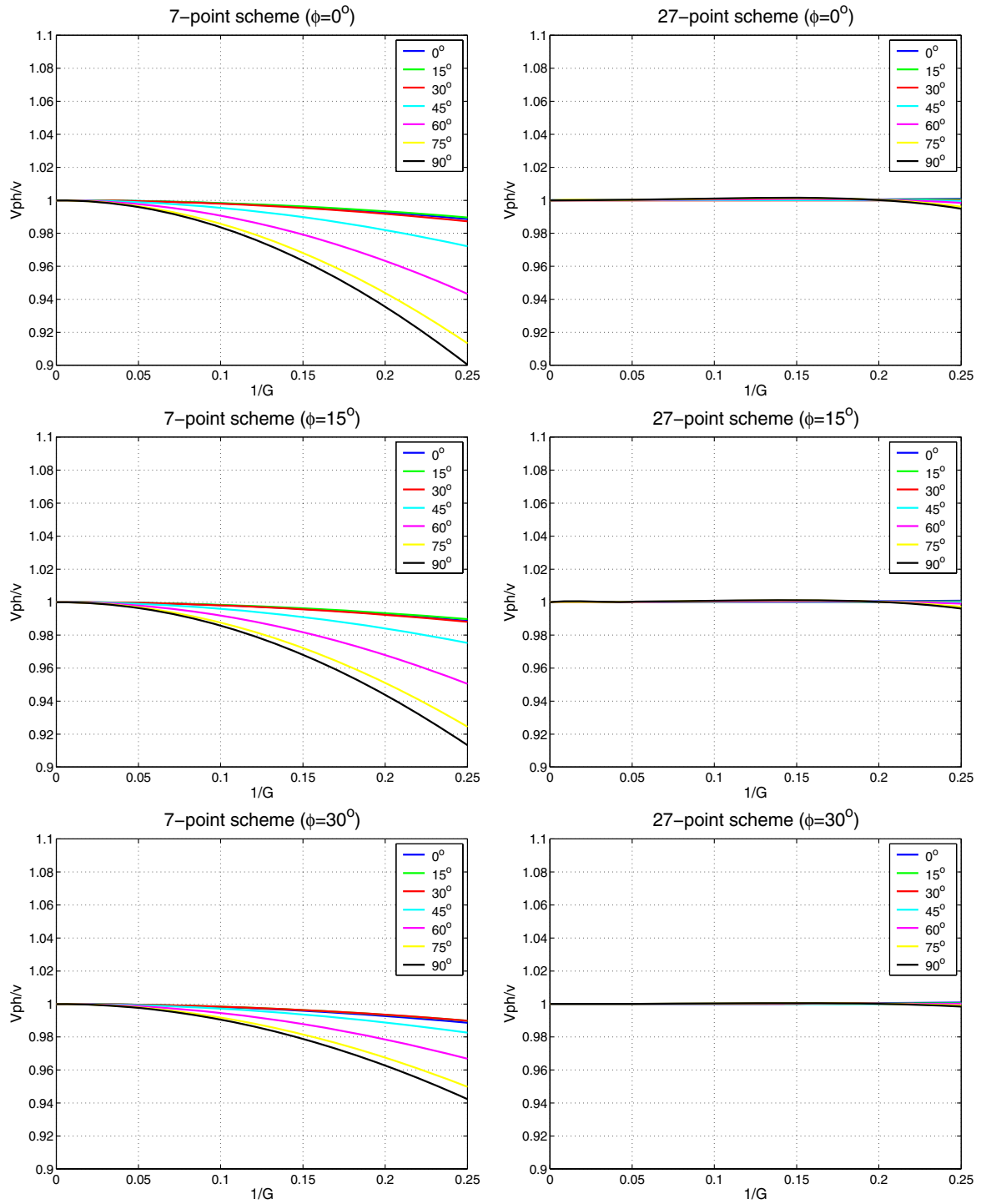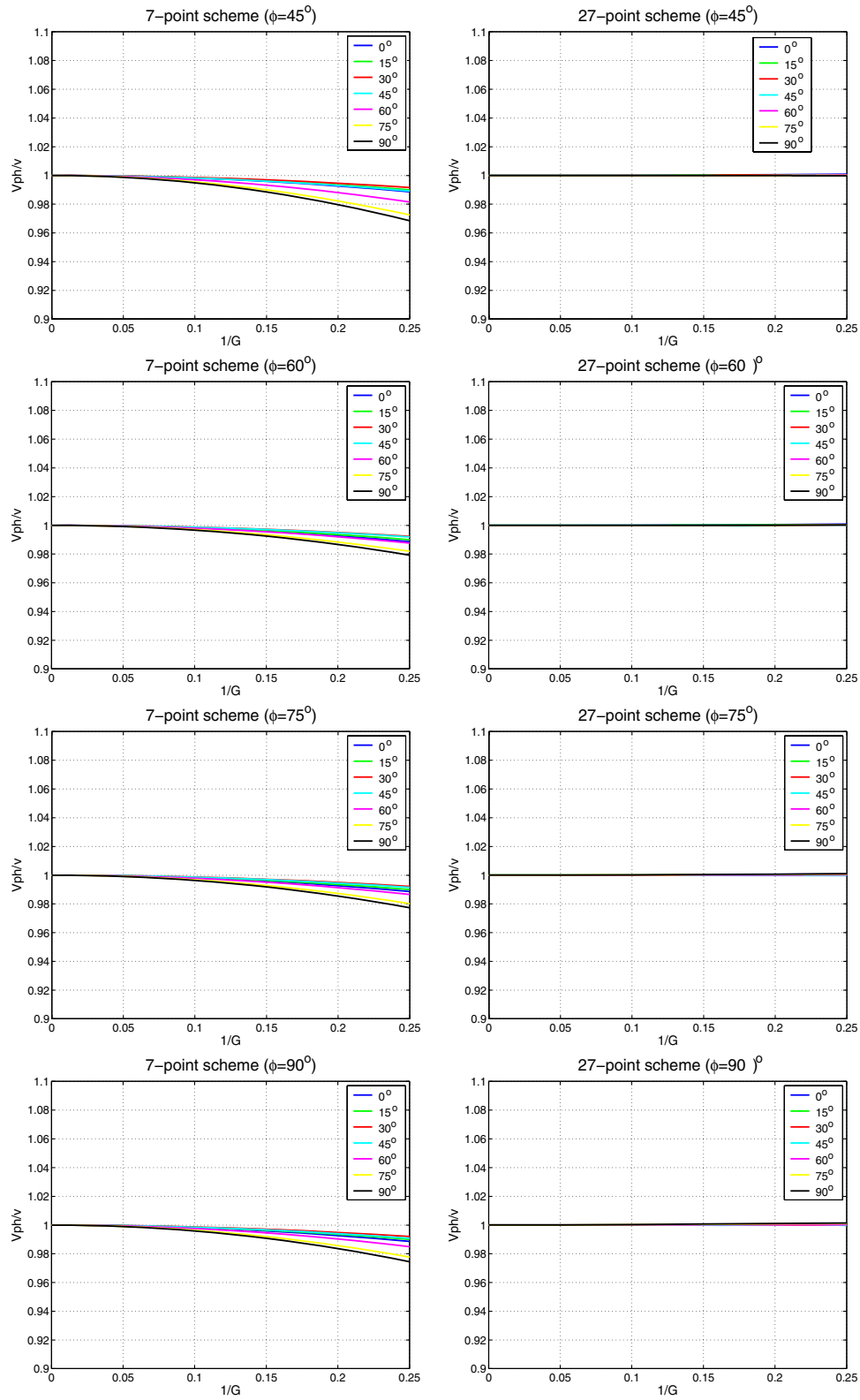
Figure 8 Continuation of Fig. 7.
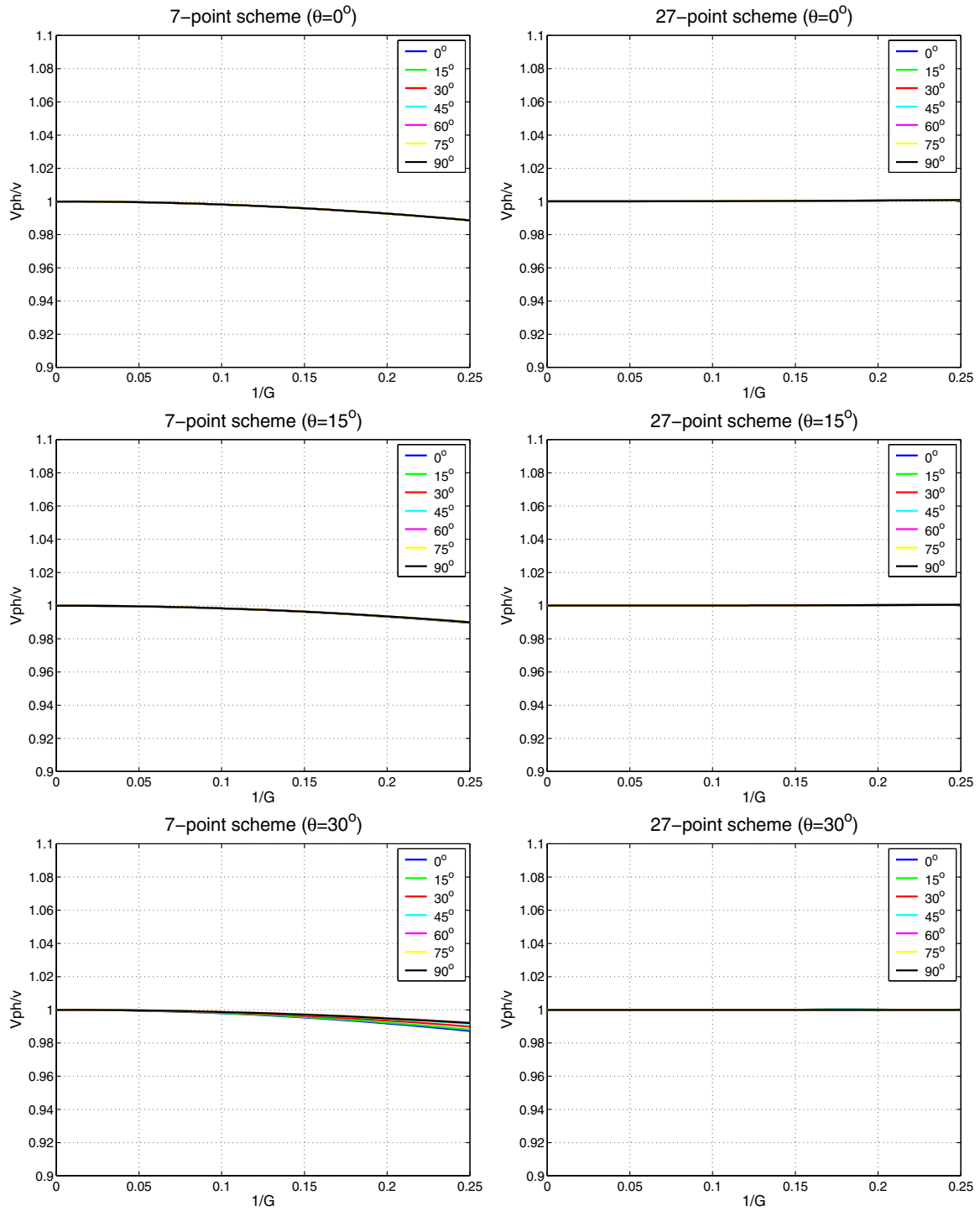
Figure 9 Normalized phase velocity curves of the classical 7-point scheme and the average-derivative optimal 27-point scheme for fixed propagation angle θ and different azimuth angles ϕ when $r_1 = 2$ and $r_2 = 3$.
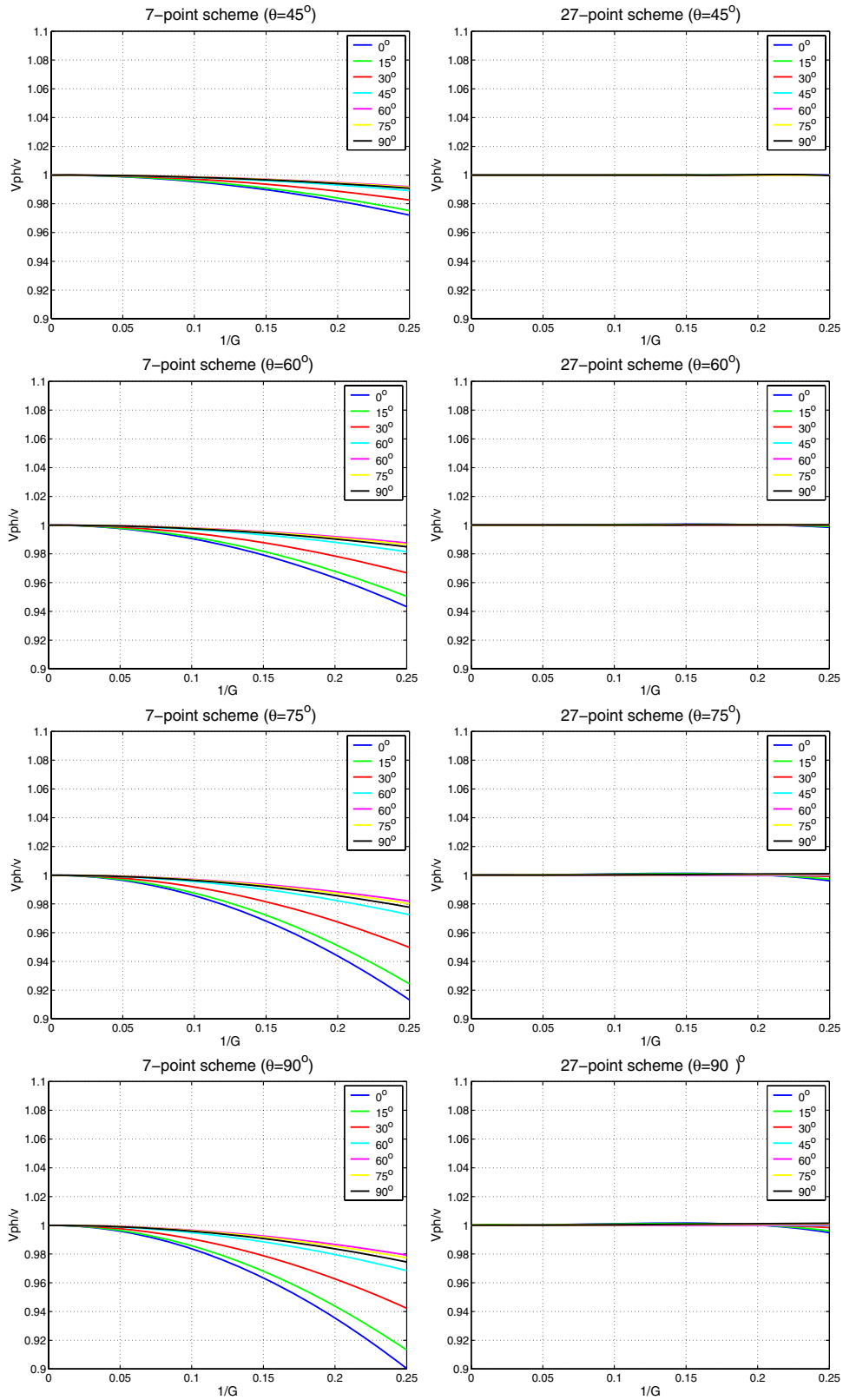
Figure 10 Continuation of Fig. 9.

(a)

(b)
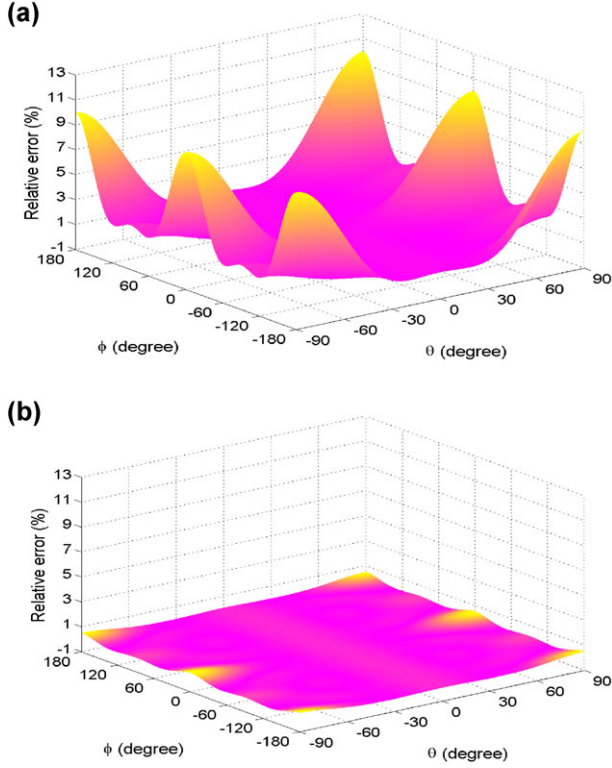
Figure 11 The relative phase velocity error for the classical 7-point scheme (a) and the average-derivative optimal 27-point scheme (b) when $r_1 = 2$ and $r_2 = 3$.

where $\rho(x, y, z)$ is the density and $\kappa(x, y, z)$ is the complex bulk modulus that accounts for attenuation in one of the following two ways:

$$\kappa(x, y, z) = \rho(x, y, z)v^2(x, y, z)\left(1 - i\frac{1}{2Q}\right)^2, \tag{9}$$

$$\frac{1}{\kappa(x, y, z)} = \frac{1}{\rho(x, y, z)}\left(\frac{1}{v(x, y, z)} + \frac{1}{\pi v(x, y, z)Q}\ln\left|\frac{\omega_r}{\omega}\right|\right.$$
$$\left. + i\frac{\mathrm{sgn}(\omega)}{2v(x, y, z)Q}\right)^2, \tag{10}$$

where $v(x, y, z)$ is the real velocity, Q is the attenuation factor, i is the unit of imaginary numbers, sgn is the sign function and ω_r is a reference frequency (Operto *et al.* 2007).

An average-derivative optimal 27-point scheme for equation (8) is

$$\frac{1}{\Delta x^2}\left[\frac{1}{\rho_{m+\frac{1}{2}, l, n}}\bar{P}_{m+1, l, n} - \left(\frac{1}{\rho_{m+\frac{1}{2}, l, n}} + \frac{1}{\rho_{m-\frac{1}{2}, l, n}}\right)\bar{P}_{m, l, n}\right.$$
$$\left. + \frac{1}{\rho_{m-\frac{1}{2}, l, n}}\bar{P}_{m-1, l, n}\right]$$
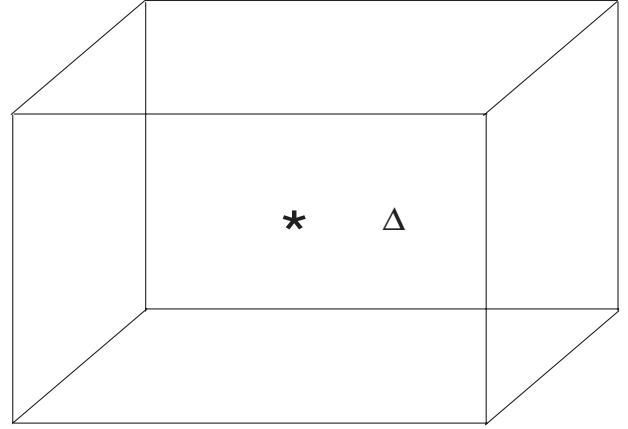
Figure 12 Schematic of the homogeneous model. The symbol * represents the source and Δ the receiver.

$$+ \frac{1}{\Delta y^2}\left[\frac{1}{\rho_{m, l+\frac{1}{2}, n}}\hat{P}_{m, l+1, n} - \left(\frac{1}{\rho_{m, l+\frac{1}{2}, n}} + \frac{1}{\rho_{m, l-\frac{1}{2}, n}}\right)\hat{P}_{m, l, n}\right.$$
$$\left. + \frac{1}{\rho_{m, l-\frac{1}{2}, n}}\hat{P}_{m, l-1, n}\right]$$
$$+ \frac{1}{\Delta z^2}\left[\frac{1}{\rho_{m, l, n+\frac{1}{2}}}\tilde{P}_{m, l, n+1} - \left(\frac{1}{\rho_{m, l, n+\frac{1}{2}}} + \frac{1}{\rho_{m, l, n-\frac{1}{2}}}\right)\tilde{P}_{m, l, n}\right.$$
$$\left. + \frac{1}{\rho_{m, l, n-\frac{1}{2}}}\tilde{P}_{m, l, n-1}\right]$$
$$+ \frac{\omega^2}{\kappa_{m, l, n}^2}\left(cP_{m, l, n} + dA + eB + fC\right) = 0, \tag{11}$$

where

$$\rho_{m+\frac{1}{2}, l, n} = \frac{1}{2}(\rho_{m, l, n} + \rho_{m+1, l, n}), \quad \rho_{m-\frac{1}{2}, l, n} = \frac{1}{2}(\rho_{m-1, l, n} + \rho_{m, l, n}),$$

$$\rho_{m, l+\frac{1}{2}, n} = \frac{1}{2}(\rho_{m, l, n} + \rho_{m, l+1, n}), \quad \rho_{m, l-\frac{1}{2}, n} = \frac{1}{2}(\rho_{m, l-1, n} + \rho_{m, l, n}),$$

$$\rho_{m, l, n+\frac{1}{2}} = \frac{1}{2}(\rho_{m, l, n} + \rho_{m, l, n+1}), \quad \rho_{m, l, n-\frac{1}{2}} = \frac{1}{2}(\rho_{m, l, n-1} + \rho_{m, l, n}).$$

NUMERICAL EXAMPLES

In this section, I present two numerical examples to verify the theoretical analysis on the classical 7-point scheme (2) and the average-derivative optimal 27-point scheme (3). First, I consider a homogeneous velocity model with a velocity of 3000 m/s (Fig. 12). In this case, an analytical solution is available to make comparisons with numerical solutions. Horizontal and vertical samplings are $nx = 51$, $ny = 51$ and $nz = 41$, respectively. A Ricker wavelet with a peak frequency of 25 Hz is placed at the centre of the model as a source and a
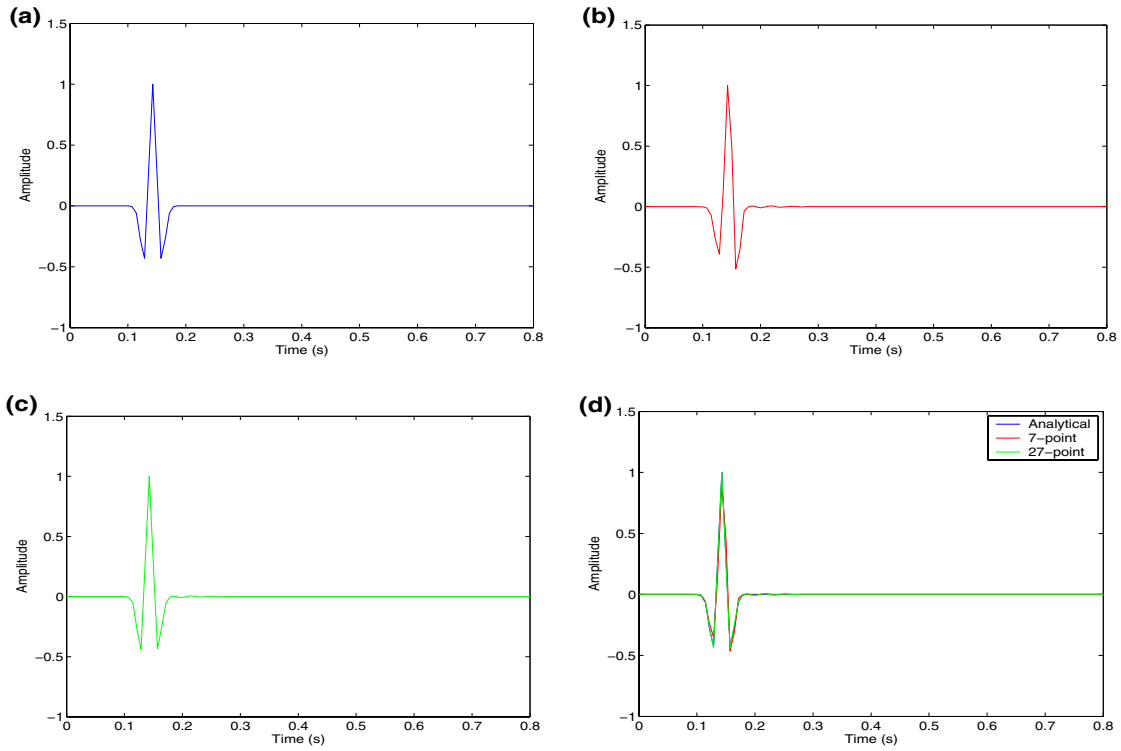
Figure 13 Seismograms computed with the analytical method (a), the classical 7-point scheme (b), the average-derivative optimal 27-point scheme (c) and the superimposed results (d). Here $r_1 = 1$ and $r_2 = 1$.
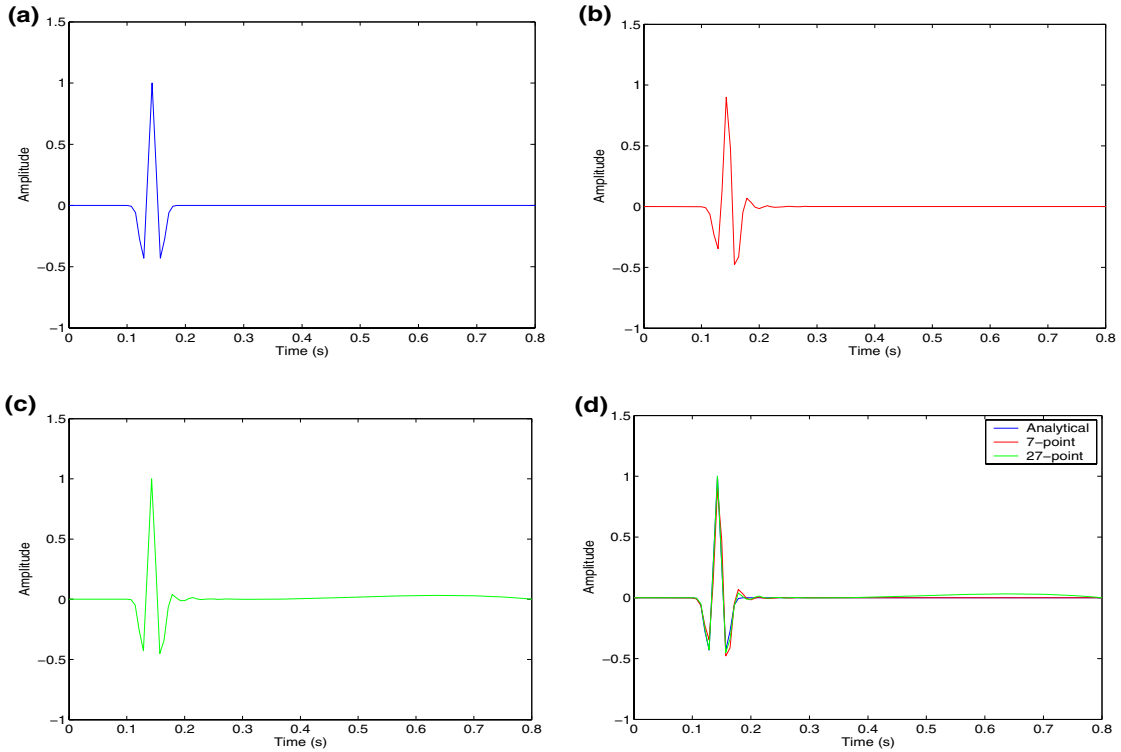
Figure 14 Seismograms computed with the analytical method (a), the classical 7-point scheme (b), the average-derivative optimal 27-point scheme (c) and the superimposed results (d). Here $r_1 = 2$ and $r_2 = 3$.

receiver is set halfway horizontally between the source and the boundary. The maximum frequency used in the computation is 70 Hz. I first consider the case where $r_1 = 1$ and $r_2 = 1$. According to the criterion of 4 grid points per smallest wavelength, horizontal sampling interval is determined by $dx = 3000/70/4$ m ≈ 11 m and $dy = dx$ and $dz = dx$.

For the analytical solution, the following formula is used:

$$P(x, y, z, t) = \mathcal{F}^{-1}\left[\frac{1}{r}\exp\left\{i\omega\frac{r}{v}\right\}\mathcal{F}(f(t))\right], \tag{12}$$

where $\mathcal{F}$ and $\mathcal{F}^{-1}$ are forward and inverse Fourier transformations with respect to time, respectively, $f(t)$ is the Ricker wavelet and

$$r = \sqrt{(x - x_0)^2 + (y - y_0)^2 + (z - z_0)^2},$$

where (x_0, y_0, z_0) is the source position.

Figure 15 Schematic of the salt dome model.
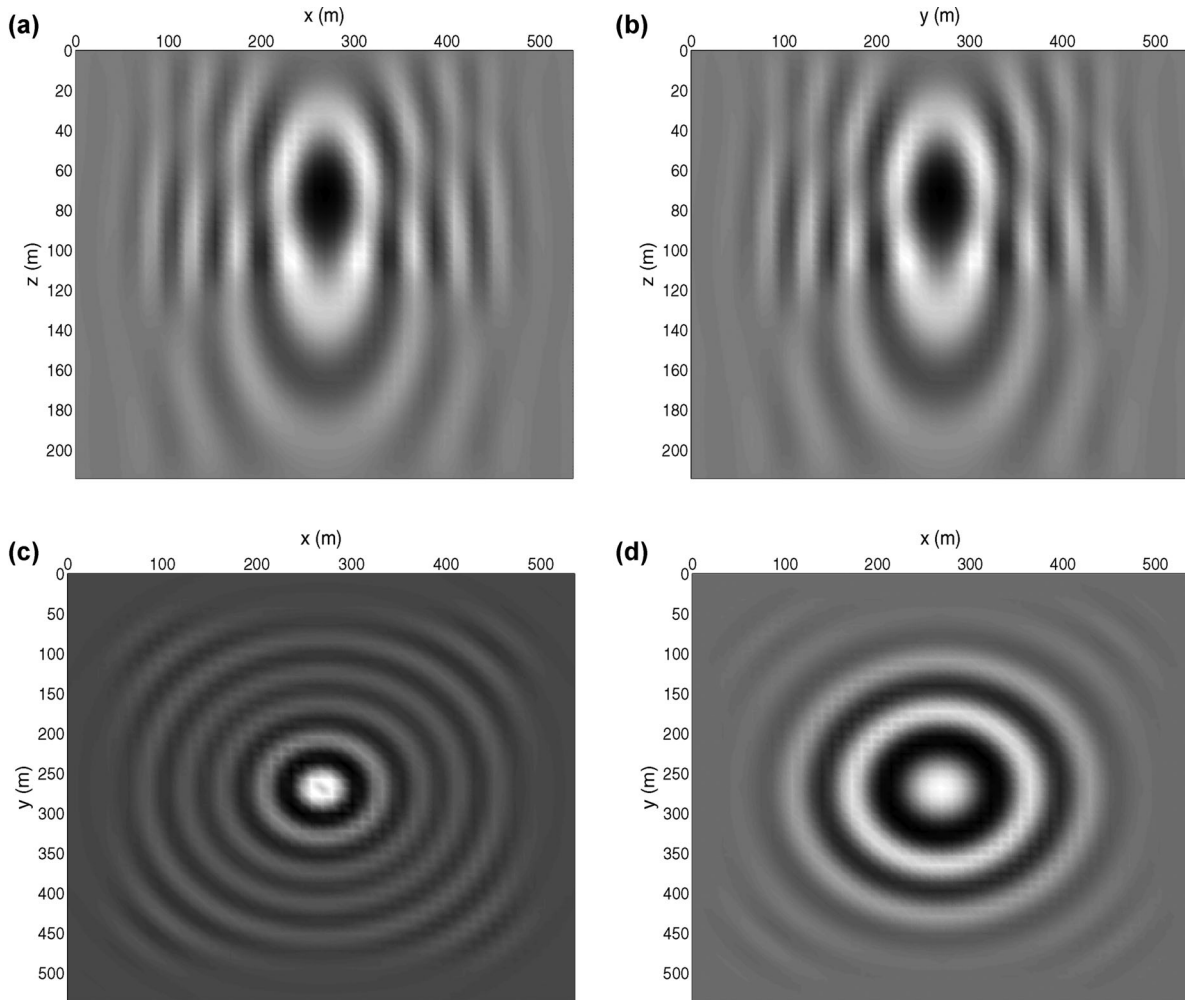
Figure 16 Sections of a 70 Hz monochromatic wavefield. Cross-line section for $y = 319$ m (a), in-line section for $x = 319$ m (b), depth section for $z = 159$ m (c) and depth section for $z = 60$ m (d).

Figure 13 shows the results computed with the analytical formula (12), the classical 7-point scheme (2) and the average-derivative optimal scheme (3). The simulation result with the average-derivative optimal 27-point scheme (3) is in good agreement with the analytical result while the result with the classical 7-point scheme (2) exhibits errors due to numerical dispersion. Figure 14 shows the results for the case where $r_1 = 2$ and $r_2 = 3$. In this case, $dx = 3000/70/4$ m ≈ 11 m and $dy = dx/2$ and $dz = dx/3$. Again, the simulation result with the average-derivative optimal 27-point scheme (3) is better than that of the classical 7-point scheme (2) in terms of agreement with the analytical result.

Second, I consider a heterogeneous velocity model and examine the performance of the average-derivative optimal 27-point scheme (3) in a heterogeneous model. Figure 15 shows a salt dome velocity model. The velocity of the salt dome is 4000 m/s and the velocity of the overburden is 3000 m/s. The sampling numbers, the Ricker wavelet and the maximum frequency used in this example are the same as those used in the homogeneous velocity model. In this example, I consider another case where $r_1 = 1$ and $r_2 = 2$. The source is placed at ($x = 275$ m, $y = 275$ m, $z = 77$ m). PML (Perfectly Matched Layer) boundary conditions are used (see Appendix) in which $L_x = L_y = L_z = 10$ and $c_x = c_y = c_z = 180$.

Figure 16 shows the sections of the 70 Hz monochromatic wavefield computed with the average-derivative optimal 27-point scheme (3). Because of the symmetry of the velocity model, the cross-line and in-line sections are basically the same. The two depth sections correspond to the positions inside and above the salt dome, respectively. No visible dispersion and boundary reflections are observed.

CONCLUSIONS

I have presented an average-derivative optimal 27-point scheme for the 3D frequency-domain wave equation in detail. The optimization coefficients are obtained by minimizing the phase velocity errors and they vary with the ratios of directional sampling intervals. Based on dispersion analysis, a conclusion is drawn that within the phase velocity error of 1% and for equal and unequal directional sampling intervals, the classical 7-point scheme requires approximately 13 grid points per shortest wavelength and the average-derivative optimal 27-point scheme requires approximately 4 grid points. Two numerical examples demonstrate the theoretical analysis. Natural generalization to the 3D viscous case and incorporation with PML boundary conditions show the great flexibility

and broad applicability of the 3D average-derivative optimal method.

REFERENCES

Boonyasiriwat, C., P. Valasek, P. Routh, W. Cao, G. T. Schuster, and B. Macy, 2009, An efficient multiscale method for time-domain waveform tomography: *Geophysics*, **74**(6), WCC59-WCC68.

Chen, J.-B., 2001, New schemes for the nonlinear Schrödinger equation: *Applied Mathematics and Computation*, **124**, 371-379.

Chen, J.-B., 2008, Variational integrators and the finite element method: *Applied Mathematics and Computation*, **196**, 941-958.

Chen, J.-B., 2009, Lax-Wendroff and Nyström methods for seismic modelling: *Geophysical Prospecting*, **57**, 931-941.

Chen, J.-B., 2012, An average-derivative optimal scheme for frequency-domain scalar wave equation: *Geophysics*, **77** (6), T201-T210.

Clapp, R. G., 2009, Reverse time migration with random boundaries: *79th Annual International Meeting, SEG, Expanded Abstracts*, 2809-2813.

Clayton, R., and B. Engqusit, 1977, Absorbing boundary conditions for scalar and elastic wave equations: *Bulletin of the Seismological Society of America*, **67**, 1529-1540.

Gauthier, O., J. Virieux, and A. Tarantola, 1986, Two-dimensional nonlinear inversion of seismic waveforms: Numerical results: *Geophysics*, **51**, 1387-1403.

Hustedt,B., S. Operto, and J. Virieux, 2004, Mix-grid and staggered-grid finite-difference methods for frquency-domain acoustic wave modelling: *Geophysical Journal International*, **157**, 1269-1296.

Jo, C.-H., C. Shin, and J. H. Suh, 1996, An optimal 9-point, finite-difference, frequency-space, 2-D scalar wave extrapolator: *Geophysics*, **61**, 529-537.

Operto, S., J. Virieux, P. Amestoy, J.-Y. L'Excellent, L. Giraud, and H. B. H. Ali, 2007, 3D finite-difference frequency-domain modeling of visco-acoustic wave propagation using a massively parallel direct solver: *A feasibility study: Geophysics*, **72**(5), SM195-SM211.

Operto, S., J. Virieux, and F. Sourbier, 2007, Documentation of FWT2D program (version 4.8): Frequency-domain full-waveform modeling/inversion of wide-aperture seismic data for imaging 2D scalar media: Technical report N° 007-SEISCOPE project.

Pratt, R. G., C. Shin, and G. J. Hicks, 1998, Gauss-Newton and full Newton methods in frequency-space seismic waveform inversion: *Geophysical Journal International*, **133**, 341-362.

Pratt, R. G., and M.-H. Worthington, 1990, Inverse theory applied to multi-source cross-hole tomography, Part I: acoustic wave-equation method: *Geophysical Prospecting*, **38**, 287-310.

Symes, W. M., 2007, Reverse-time migration with optimal checkpointing: *Geophysics*, **72**(5), SM213-SM221.

Tarantola, A., 1984, Inversion of seismic reflection data in the acoustic approximation: *Geophysics*, **49**, 1259-1266.

Virieux, J., and S. Operto, 2009, An overview of full-waveform inversion in exploration geophysics: *Geophysics*, **74**(6), WCC1-WCC26.

APPENDIX

COEFFICIENTS WITH PERFECTLY MATCHED LAYER BOUNDARY CONDITIONS FOR THE AVERAGE-DERIVATIVE 27-POINT SCHEME

The 3D frequency-domain scalar wave equation with PML boundary conditions reads:

$$\frac{1}{\xi_x}\frac{\partial}{\partial x}\left(\frac{1}{\xi_x}\frac{\partial P}{\partial x}\right) + \frac{1}{\xi_y}\frac{\partial}{\partial y}\left(\frac{1}{\xi_y}\frac{\partial P}{\partial y}\right) + \frac{1}{\xi_z}\frac{\partial}{\partial z}\left(\frac{1}{\xi_z}\frac{\partial P}{\partial z}\right)$$

$$+ \frac{\omega^2}{v^2}P = 0, \tag{A1}$$

where

$$\xi_x(x) = 1 - \frac{i c_x}{\omega}\cos\left(\frac{\pi}{2}\frac{x}{L_x}\right), \tag{A2}$$

$$\xi_y(z) = 1 - \frac{i c_y}{\omega}\cos\left(\frac{\pi}{2}\frac{y}{L_y}\right), \tag{A3}$$

$$\xi_z(z) = 1 - \frac{i c_z}{\omega}\cos\left(\frac{\pi}{2}\frac{z}{L_z}\right), \tag{A4}$$

where L_x, L_y, and L_z denote the width of the PML layer in the x- y- and z-directions, respectively. The coordinates x, y, and z are local coordinates whose origins are located at the outer edges of the PML layers. The scalars c_x, c_y and c_z depend on L_x, L_y, and L_z, respectively and are determined by trial and error (Operto *et al.* 2007). For a function $f(t)$ in time, its Fourier $\mathcal{F}(\omega)$ is defined as:

$$\mathcal{F}(\omega) = \int f(t)e^{-i\omega t}\,dt. \tag{A5}$$

If one uses another definition:

$$\mathcal{F}(\omega) = \int f(t)e^{i\omega t}\,dt, \tag{A6}$$

then ω in equations (A2)–(A4) should be replaced by $-\omega$.

The average-derivative optimal 27-point scheme for equation (A1) becomes:

$$\frac{1}{\xi_{x_m}}\frac{1}{\Delta x^2}\left[\frac{1}{\xi_{x_{m+\frac{1}{2}}}}\bar{P}_{m+1,l,n} - \left(\frac{1}{\xi_{x_{m+\frac{1}{2}}}} + \frac{1}{\xi_{x_{m-\frac{1}{2}}}}\right)\bar{P}_{m,l,n}\right.$$

$$\left. + \frac{1}{\xi_{x_{m-\frac{1}{2}}}}\bar{P}_{m-1,l,n}\right]$$

$$+ \frac{1}{\xi_{y_l}}\frac{1}{\Delta y^2}\left[\frac{1}{\xi_{y_{l+\frac{1}{2}}}}\hat{P}_{m,l+1,n} - \left(\frac{1}{\xi_{y_{l+\frac{1}{2}}}} + \frac{1}{\xi_{y_{l-\frac{1}{2}}}}\right)\hat{P}_{m,l,n}\right.$$

$$\left. + \frac{1}{\xi_{y_{l-\frac{1}{2}}}}\hat{P}_{m,l-1,n}\right]$$

$$+ \frac{1}{\xi_{z_n}}\frac{1}{\Delta z^2}\left[\frac{1}{\xi_{z_{n+\frac{1}{2}}}}\tilde{P}_{m,l,n+1} - \left(\frac{1}{\xi_{z_{n+\frac{1}{2}}}} + \frac{1}{\xi_{z_{n-\frac{1}{2}}}}\right)\tilde{P}_{m,l,n}\right.$$

$$\left. + \frac{1}{\xi_{z_{n-\frac{1}{2}}}}\tilde{P}_{m,l,n-1}\right]$$

$$+ \frac{\omega^2}{v^2_{m,l,n}}\left(c P_{m,l,n} + dA + eB + fC\right) = 0, \tag{A7}$$

where

$$\xi_{x_{m+\frac{1}{2}}} = \frac{1}{2}(\xi_{x_m} + \xi_{x_{m+1}}), \quad \xi_{x_{m-\frac{1}{2}}} = \frac{1}{2}(\xi_{x_{m-1}} + \xi_{x_m}),$$

$$\xi_{y_{l+\frac{1}{2}}} = \frac{1}{2}(\xi_{y_l} + \xi_{y_{l+1}}), \quad \xi_{y_{l-\frac{1}{2}}} = \frac{1}{2}(\xi_{y_{l-1}} + \xi_{y_l}),$$

$$\xi_{z_{n+\frac{1}{2}}} = \frac{1}{2}(\xi_{z_n} + \xi_{z_{n+1}}), \quad \xi_{z_{n-\frac{1}{2}}} = \frac{1}{2}(\xi_{z_{n-1}} + \xi_{z_n}).$$

Using the ordering in Fig. A1, scheme (A7) can be rewritten as:

$$c_1 P_{m-1,l-1,n-1} + c_2 P_{m,l-1,n-1} + c_3 P_{m+1,l-1,n-1} + c_4 P_{m-1,l,n-1}$$

$$+ c_5 P_{m,l,n-1} + c_6 P_{m+1,l,n-1} + c_7 P_{m-1,l+1,n-1} + c_8 P_{m,l+1,n-1}$$

$$+ c_9 P_{m+1,l+1,n-1} + c_{10} P_{m-1,l-1,n} + c_{11} P_{m,l-1,n}$$

$$+ c_{12} P_{m+1,l-1,n} + c_{13} P_{m-1,l,n} + c_{14} P_{m,l,n} + c_{15} P_{m+1,l,n} +$$

$$+ c_{16} P_{m-1,l+1,n} + c_{17} P_{m,l+1,n} + c_{18} P_{m+1,l+1,n}$$

$$+ c_{19} P_{m-1,l-1,n+1} + c_{20} P_{m,l-1,n+1} + c_{21} P_{m+1,l-1,n+1}$$

$$+ c_{22} P_{m-1,l,n+1} + c_{23} P_{m,l,n+1} + c_{24} P_{m+1,l,n+1} \tag{A8}$$

$$+ c_{25} P_{m-1,l+1,n+1} + c_{26} P_{m,l+1,n+1} + c_{27} P_{m+1,l+1,n+1} = 0,$$

where

$$c_1 = \frac{1}{\xi_{x_m}}\frac{1}{\xi_{x_{m-\frac{1}{2}}}}\frac{\alpha_2}{\Delta x^2} + \frac{1}{\xi_{y_l}}\frac{1}{\xi_{y_{l-\frac{1}{2}}}}\frac{\beta_2}{\Delta y^2} + \frac{1}{\xi_{z_n}}\frac{1}{\xi_{z_{n-\frac{1}{2}}}}\frac{\gamma_2}{\Delta z^2} + f\frac{\omega^2}{v^2_{m,l,n}},$$

$$c_2 = -\frac{1}{\xi_{x_m}}\left(\frac{1}{\xi_{x_{m+\frac{1}{2}}}} + \frac{1}{\xi_{x_{m-\frac{1}{2}}}}\right)\frac{\alpha_2}{\Delta x^2} + \frac{1}{\xi_{y_l}}\frac{1}{\xi_{y_{l-\frac{1}{2}}}}\frac{\beta_1}{\Delta y^2}$$

$$+ \frac{1}{\xi_{z_n}}\frac{1}{\xi_{z_{n-\frac{1}{2}}}}\frac{\gamma_1}{\Delta z^2} + e\frac{\omega^2}{v^2_{m,l,n}},$$

$$c_3 = \frac{1}{\xi_{x_m}}\frac{1}{\xi_{x_{m+\frac{1}{2}}}}\frac{\alpha_2}{\Delta x^2} + \frac{1}{\xi_{y_l}}\frac{1}{\xi_{y_{l-\frac{1}{2}}}}\frac{\beta_2}{\Delta y^2} + \frac{1}{\xi_{z_n}}\frac{1}{\xi_{z_{n-\frac{1}{2}}}}\frac{\gamma_2}{\Delta z^2} + f\frac{\omega^2}{v_{m,l,n}^2},$$

$$c_4 = \frac{1}{\xi_{x_m}}\frac{1}{\xi_{x_{m-\frac{1}{2}}}}\frac{\alpha_1}{\Delta x^2} - \frac{1}{\xi_{y_l}}\left(\frac{1}{\xi_{y_{l+\frac{1}{2}}}} + \frac{1}{\xi_{y_{l-\frac{1}{2}}}}\right)\frac{\beta_2}{\Delta y^2}$$
$$+ \frac{1}{\xi_{z_n}}\frac{1}{\xi_{z_{n-\frac{1}{2}}}}\frac{\gamma_1}{\Delta z^2} + e\frac{\omega^2}{v_{m,l,n}^2},$$

$$c_5 = -\frac{1}{\xi_{x_m}}\left(\frac{1}{\xi_{x_{m+\frac{1}{2}}}} + \frac{1}{\xi_{x_{m-\frac{1}{2}}}}\right)\frac{\alpha_1}{\Delta x^2} - \frac{1}{\xi_{y_l}}\left(\frac{1}{\xi_{y_{l+\frac{1}{2}}}} + \frac{1}{\xi_{y_{l-\frac{1}{2}}}}\right)$$
$$\times \frac{\beta_1}{\Delta y^2} + \frac{1}{\xi_{z_n}}\frac{1}{\xi_{z_{n-\frac{1}{2}}}}\frac{1-4\gamma_1-4\gamma_2}{\Delta z^2} + d\frac{\omega^2}{v_{m,l,n}^2},$$

$$c_6 = \frac{1}{\xi_{x_m}}\frac{1}{\xi_{x_{m+\frac{1}{2}}}}\frac{\alpha_1}{\Delta x^2} - \frac{1}{\xi_{y_l}}\left(\frac{1}{\xi_{y_{l+\frac{1}{2}}}} + \frac{1}{\xi_{y_{l-\frac{1}{2}}}}\right)\frac{\beta_2}{\Delta y^2}$$
$$+ \frac{1}{\xi_{z_n}}\frac{1}{\xi_{z_{n-\frac{1}{2}}}}\frac{\gamma_1}{\Delta z^2} + e\frac{\omega^2}{v_{m,l,n}^2},$$

$$c_7 = \frac{1}{\xi_{x_m}}\frac{1}{\xi_{x_{m-\frac{1}{2}}}}\frac{\alpha_2}{\Delta x^2} + \frac{1}{\xi_{y_l}}\frac{1}{\xi_{y_{l+\frac{1}{2}}}}\frac{\beta_2}{\Delta y^2} + \frac{1}{\xi_{z_n}}\frac{1}{\xi_{z_{n-\frac{1}{2}}}}\frac{\gamma_2}{\Delta z^2} + f\frac{\omega^2}{v_{m,l,n}^2},$$

$$c_8 = -\frac{1}{\xi_{x_m}}\left(\frac{1}{\xi_{x_{m+\frac{1}{2}}}} + \frac{1}{\xi_{x_{m-\frac{1}{2}}}}\right)\frac{\alpha_2}{\Delta x^2} + \frac{1}{\xi_{y_l}}\frac{1}{\xi_{y_{l+\frac{1}{2}}}}\frac{\beta_1}{\Delta y^2}$$
$$+ \frac{1}{\xi_{z_n}}\frac{1}{\xi_{z_{n-\frac{1}{2}}}}\frac{\gamma_1}{\Delta z^2} + e\frac{\omega^2}{v_{m,l,n}^2},$$

$$c_9 = \frac{1}{\xi_{x_m}}\frac{1}{\xi_{x_{m+\frac{1}{2}}}}\frac{\alpha_2}{\Delta x^2} + \frac{1}{\xi_{y_l}}\frac{1}{\xi_{y_{l+\frac{1}{2}}}}\frac{\beta_2}{\Delta y^2} + \frac{1}{\xi_{z_n}}\frac{1}{\xi_{z_{n-\frac{1}{2}}}}\frac{\gamma_2}{\Delta z^2} + f\frac{\omega^2}{v_{m,l,n}^2},$$

$$c_{10} = \frac{1}{\xi_{x_m}}\frac{1}{\xi_{x_{m-\frac{1}{2}}}}\frac{\alpha_1}{\Delta x^2} + \frac{1}{\xi_{y_l}}\frac{1}{\xi_{y_{l-\frac{1}{2}}}}\frac{\beta_1}{\Delta y^2}$$
$$- \frac{1}{\xi_{z_n}}\left(\frac{1}{\xi_{z_{n+\frac{1}{2}}}} + \frac{1}{\xi_{z_{n-\frac{1}{2}}}}\right)\frac{\gamma_2}{\Delta z^2} + e\frac{\omega^2}{v_{m,l,n}^2},$$

$$c_{11} = -\frac{1}{\xi_{x_m}}\left(\frac{1}{\xi_{x_{m+\frac{1}{2}}}} + \frac{1}{\xi_{x_{m-\frac{1}{2}}}}\right)\frac{\alpha_1}{\Delta x^2} + \frac{1}{\xi_{y_l}}\frac{1}{\xi_{y_{l-\frac{1}{2}}}}\frac{1-4\beta_1-4\beta_2}{\Delta y^2}$$
$$- \frac{1}{\xi_{z_n}}\left(\frac{1}{\xi_{z_{n+\frac{1}{2}}}} + \frac{1}{\xi_{z_{n-\frac{1}{2}}}}\right)\frac{\gamma_1}{\Delta z^2} + d\frac{\omega^2}{v_{m,l,n}^2},$$

$$c_{12} = \frac{1}{\xi_{x_m}}\frac{1}{\xi_{x_{m+\frac{1}{2}}}}\frac{\alpha_1}{\Delta x^2} + \frac{1}{\xi_{y_l}}\frac{1}{\xi_{y_{l-\frac{1}{2}}}}\frac{\beta_1}{\Delta y^2}$$
$$- \frac{1}{\xi_{z_n}}\left(\frac{1}{\xi_{z_{n+\frac{1}{2}}}} + \frac{1}{\xi_{z_{n-\frac{1}{2}}}}\right)\frac{\gamma_2}{\Delta z^2} + e\frac{\omega^2}{v_{m,l,n}^2},$$

$$c_{13} = \frac{1}{\xi_{x_m}}\frac{1}{\xi_{x_{m-\frac{1}{2}}}}\frac{1-4\alpha_1-4\alpha_2}{\Delta x^2} - \frac{1}{\xi_{y_l}}\left(\frac{1}{\xi_{y_{l+\frac{1}{2}}}} + \frac{1}{\xi_{y_{l-\frac{1}{2}}}}\right)\frac{\beta_1}{\Delta y^2}$$
$$- \frac{1}{\xi_{z_n}}\left(\frac{1}{\xi_{z_{n+\frac{1}{2}}}} + \frac{1}{\xi_{z_{n-\frac{1}{2}}}}\right)\frac{\gamma_1}{\Delta z^2} + d\frac{\omega^2}{v_{m,l,n}^2},$$

$$c_{14} = -\frac{1}{\xi_{x_m}}\left(\frac{1}{\xi_{x_{m+\frac{1}{2}}}} + \frac{1}{\xi_{x_{m-\frac{1}{2}}}}\right)\frac{1-4\alpha_1-4\alpha_2}{\Delta x^2}$$

$$- \frac{1}{\xi_{y_l}}\left(\frac{1}{\xi_{y_{l+\frac{1}{2}}}} + \frac{1}{\xi_{y_{l-\frac{1}{2}}}}\right)\frac{1-4\beta_1-4\beta_2}{\Delta y^2}$$
$$- \frac{1}{\xi_{z_n}}\left(\frac{1}{\xi_{z_{n+\frac{1}{2}}}} + \frac{1}{\xi_{z_{n-\frac{1}{2}}}}\right)\frac{1-4\gamma_1-4\gamma_2}{\Delta z^2} + c\frac{\omega^2}{v_{m,l,n}^2},$$

$$c_{15} = \frac{1}{\xi_{x_m}}\frac{1}{\xi_{x_{m+\frac{1}{2}}}}\frac{1-4\alpha_1-4\alpha_2}{\Delta x^2} - \frac{1}{\xi_{y_l}}\left(\frac{1}{\xi_{y_{l+\frac{1}{2}}}} + \frac{1}{\xi_{y_{l-\frac{1}{2}}}}\right)\frac{\beta_1}{\Delta y^2}$$
$$- \frac{1}{\xi_{z_n}}\left(\frac{1}{\xi_{z_{n+\frac{1}{2}}}} + \frac{1}{\xi_{z_{n-\frac{1}{2}}}}\right)\frac{\gamma_1}{\Delta z^2} + d\frac{\omega^2}{v_{m,l,n}^2},$$

$$c_{16} = \frac{1}{\xi_{x_m}}\frac{1}{\xi_{x_{m-\frac{1}{2}}}}\frac{\alpha_1}{\Delta x^2} + \frac{1}{\xi_{y_l}}\frac{1}{\xi_{y_{l+\frac{1}{2}}}}\frac{\beta_1}{\Delta y^2}$$
$$- \frac{1}{\xi_{z_n}}\left(\frac{1}{\xi_{z_{n+\frac{1}{2}}}} + \frac{1}{\xi_{z_{n-\frac{1}{2}}}}\right)\frac{\gamma_2}{\Delta z^2} + e\frac{\omega^2}{v_{m,l,n}^2},$$

$$c_{17} = -\frac{1}{\xi_{x_m}}\left(\frac{1}{\xi_{x_{m+\frac{1}{2}}}} + \frac{1}{\xi_{x_{m-\frac{1}{2}}}}\right)\frac{\alpha_1}{\Delta x^2} + \frac{1}{\xi_{y_l}}\frac{1}{\xi_{y_{l+\frac{1}{2}}}}\frac{1-4\beta_1-4\beta_2}{\Delta y^2}$$
$$- \frac{1}{\xi_{z_n}}\left(\frac{1}{\xi_{z_{n+\frac{1}{2}}}} + \frac{1}{\xi_{z_{n-\frac{1}{2}}}}\right)\frac{\gamma_1}{\Delta z^2} + d\frac{\omega^2}{v_{m,l,n}^2},$$

$$c_{18} = \frac{1}{\xi_{x_m}}\frac{1}{\xi_{x_{m+\frac{1}{2}}}}\frac{\alpha_1}{\Delta x^2} + \frac{1}{\xi_{y_l}}\frac{1}{\xi_{y_{l+\frac{1}{2}}}}\frac{\beta_1}{\Delta y^2}$$
$$- \frac{1}{\xi_{z_n}}\left(\frac{1}{\xi_{z_{n+\frac{1}{2}}}} + \frac{1}{\xi_{z_{n-\frac{1}{2}}}}\right)\frac{\gamma_2}{\Delta z^2} + e\frac{\omega^2}{v_{m,l,n}^2},$$

$$c_{19} = \frac{1}{\xi_{x_m}}\frac{1}{\xi_{x_{m-\frac{1}{2}}}}\frac{\alpha_2}{\Delta x^2} + \frac{1}{\xi_{y_l}}\frac{1}{\xi_{y_{l-\frac{1}{2}}}}\frac{\beta_2}{\Delta y^2} + \frac{1}{\xi_{z_n}}\frac{1}{\xi_{z_{n+\frac{1}{2}}}}\frac{\gamma_2}{\Delta z^2} + f\frac{\omega^2}{v_{m,l,n}^2},$$

$$c_{20} = -\frac{1}{\xi_{x_m}}\left(\frac{1}{\xi_{x_{m+\frac{1}{2}}}} + \frac{1}{\xi_{x_{m-\frac{1}{2}}}}\right)\frac{\alpha_2}{\Delta x^2} + \frac{1}{\xi_{y_l}}\frac{1}{\xi_{y_{l-\frac{1}{2}}}}\frac{\beta_1}{\Delta y^2}$$
$$+ \frac{1}{\xi_{z_n}}\frac{1}{\xi_{z_{n+\frac{1}{2}}}}\frac{\gamma_1}{\Delta z^2} + e\frac{\omega^2}{v_{m,l,n}^2},$$

$$c_{21} = \frac{1}{\xi_{x_m}}\frac{1}{\xi_{x_{m+\frac{1}{2}}}}\frac{\alpha_2}{\Delta x^2} + \frac{1}{\xi_{y_l}}\frac{1}{\xi_{y_{l-\frac{1}{2}}}}\frac{\beta_2}{\Delta y^2} + \frac{1}{\xi_{z_n}}\frac{1}{\xi_{z_{n+\frac{1}{2}}}}\frac{\gamma_2}{\Delta z^2} + f\frac{\omega^2}{v_{m,l,n}^2},$$

$$c_{22} = \frac{1}{\xi_{x_m}}\frac{1}{\xi_{x_{m-\frac{1}{2}}}}\frac{\alpha_1}{\Delta x^2} - \frac{1}{\xi_{y_l}}\left(\frac{1}{\xi_{y_{l+\frac{1}{2}}}} + \frac{1}{\xi_{y_{l-\frac{1}{2}}}}\right)\frac{\beta_2}{\Delta y^2}$$
$$+ \frac{1}{\xi_{z_n}}\frac{1}{\xi_{z_{n+\frac{1}{2}}}}\frac{\gamma_1}{\Delta z^2} + e\frac{\omega^2}{v_{m,l,n}^2},$$

$$c_{23} = -\frac{1}{\xi_{x_m}}\left(\frac{1}{\xi_{x_{m+\frac{1}{2}}}} + \frac{1}{\xi_{x_{m-\frac{1}{2}}}}\right)\frac{\alpha_1}{\Delta x^2} - \frac{1}{\xi_{y_l}}\left(\frac{1}{\xi_{y_{l+\frac{1}{2}}}} + \frac{1}{\xi_{y_{l-\frac{1}{2}}}}\right)$$
$$\times \frac{\beta_1}{\Delta y^2} + \frac{1}{\xi_{z_n}}\frac{1}{\xi_{z_{n+\frac{1}{2}}}}\frac{1-4\gamma_1-4\gamma_2}{\Delta z^2} + d\frac{\omega^2}{v_{m,l,n}^2},$$

$$c_{24} = \frac{1}{\xi_{x_m}}\frac{1}{\xi_{x_{m+\frac{1}{2}}}}\frac{\alpha_1}{\Delta x^2} - \frac{1}{\xi_{y_l}}\left(\frac{1}{\xi_{y_{l+\frac{1}{2}}}} + \frac{1}{\xi_{y_{l-\frac{1}{2}}}}\right)\frac{\beta_2}{\Delta y^2}$$
$$+ \frac{1}{\xi_{z_n}}\frac{1}{\xi_{z_{n+\frac{1}{2}}}}\frac{\gamma_1}{\Delta z^2} + e\frac{\omega^2}{v_{m,l,n}^2},$$

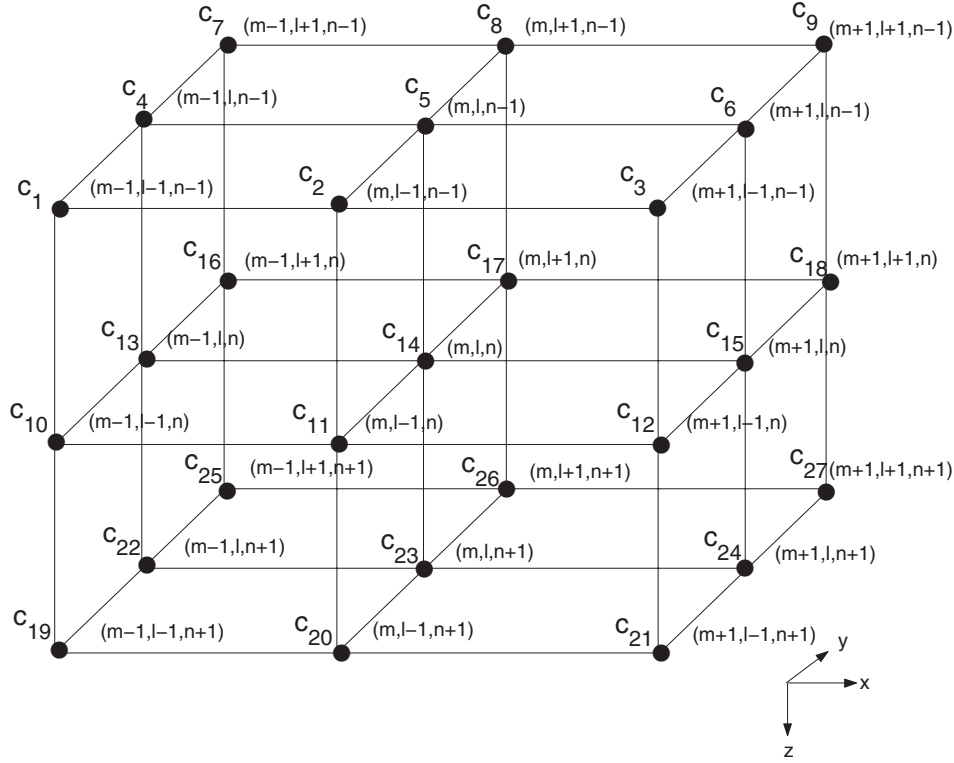**Figure A1** Schematic of the average-derivative optimal 27-point scheme and its coefficients with PML boundary conditions.

$$c_{25} = \frac{1}{\xi_{x_m}} \frac{1}{\xi_{x_{m-\frac{1}{2}}}} \frac{\alpha_2}{\Delta x^2} + \frac{1}{\xi_{y_l}} \frac{1}{\xi_{y_{l+\frac{1}{2}}}} \frac{\beta_2}{\Delta y^2} + \frac{1}{\xi_{z_n}} \frac{1}{\xi_{z_{n+\frac{1}{2}}}} \frac{\gamma_2}{\Delta z^2} + f \frac{\omega^2}{v_{m,l,n}^2},$$

$$c_{26} = -\frac{1}{\xi_{x_m}} \left(\frac{1}{\xi_{x_{m+\frac{1}{2}}}} + \frac{1}{\xi_{x_{m-\frac{1}{2}}}} \right) \frac{\alpha_2}{\Delta x^2} + \frac{1}{\xi_{y_l}} \frac{1}{\xi_{y_{l+\frac{1}{2}}}} \frac{\beta_1}{\Delta y^2}$$

$$+ \frac{1}{\xi_{z_n}} \frac{1}{\xi_{z_{n+\frac{1}{2}}}} \frac{\gamma_1}{\Delta z^2} + e \frac{\omega^2}{v_{m,l,n}^2},$$

$$c_{27} = \frac{1}{\xi_{x_m}} \frac{1}{\xi_{x_{m+\frac{1}{2}}}} \frac{\alpha_2}{\Delta x^2} + \frac{1}{\xi_{y_l}} \frac{1}{\xi_{y_{l+\frac{1}{2}}}} \frac{\beta_2}{\Delta y^2} + \frac{1}{\xi_{z_n}} \frac{1}{\xi_{z_{n+\frac{1}{2}}}} \frac{\gamma_2}{\Delta z^2} + f \frac{\omega^2}{v_{m,l,n}^2}.$$